Tectonophysics xxx (2015) xxx–xxx

Contents lists available at ScienceDirect

Tectonophysics

journal homepage: www.elsevier.com/locate/tecto

Middle to late Miocene extensional collapse of the North Patagonian Andes (41°30′–42°S)

Jonathan E. Tobal [a], Andrés Folguera [a], Jeremías Likerman [a], Maximiliano Naipauer [a], Daniel Sellés [b], Florencia L. Boedo [a], Víctor A. Ramos [a], Mario Gimenez [c]

[a] Instituto de Estudios Andinos "Don Pablo Groeber" (IDEAN), CONICET-Universidad de Buenos Aires, Argentina
[b] Aurum Consultores, Santiago, Chile
[c] Instituto Geofisico Sismologico Ing. Volponi, Universidad Nacional de San Juan, Argentina

ARTICLE INFO

Article history:
Received 15 December 2014
Received in revised form 2 June 2015
Accepted 13 June 2015
Available online xxxx

Keywords:
North Patagonian Andes
Volcanism
Hinterland extensional tectonics
Fold and thrust belt

ABSTRACT

The hinterland zone of the North Patagonian Andes between 41° and 43°S constitutes a poorly explored sector of the Andes, where no structural studies and scarce geochronological determinations have been carried out. This paper focuses on two isolated volcanic sections hosted at the main Andes, in which field evidence indicates a common synextensional origin. Geochronological data establish that this volcanic event occurred diachronously at the innermost sector of the evolving fold and thrust belt, during middle to late Miocene times. Therefore, the event was briefly coeval and postdated compressive tectonics recognized in the deformational front and correlative to the last phase of pluton emplacement of the North Patagonian Batholith. Local-scale topographic swath profiles performed in this work reveal negative topographic anomalies where normal faults were recognized. Moreover, regional swath profiles show not only a conspicuous depressed zone at the hinterland zone, where the studied sections are located, but also anomalously high altitudes at the foreland zone. In addition, calculated orogenic volumes increase in this sector of the fold and thrust belt, which agrees with recent shortening estimations. These topographic along-strike variations, in association with late Miocene extension following the main compressive stage in the area, are explained by a supercritical stage of the orogenic wedge that would have led to focused extension at the innermost sector of the fold and thrust belt.

1. Introduction

As was recently stated by Wells et al. (2012), extension within orogenic belts is a rather common process during orogenesis. Moreover, extensional deformation during plate convergence is observed in elevated hinterlands of ancient and present fold thrust belts all around the world (e.g., the eastern Alps, the Apennines, the Calabria Arc, the Himalayas, the Scandinavian Caledonides, the Sevier–Laramide orogen, among others; for a synthesis see Wells and Hoisch, 2008, and references therein). Among the few examples of active hinterland extension, the Cordillera Blanca of Peru in the Andes of South America, probably constitutes one of the most outstanding examples of active large-scale extension within the hinterland in a subduction setting (Giovanni et al., 2010; McNulty and Farber, 2002). Even though there is a large amount of studies focused on this subject, the processes that drive extensional tectonics at the hinterland during convergence remain poorly understood and are still matter of debate (see Wells et al., 2012 for a review).

In the North Patagonian Andes, over the western Ñirihuau fold and thrust belt (Bechis and Cristallini, 2006; Giacosa and Heredia, 2004; Giacosa et al., 2005; Orts et al., 2012; Ramos and Cortés, 1984), two isolated volcanic sections were previously attributed to the Oligocene (El Maitén belt; Rapela et al., 1988). However, neither field nor previous geochronological data support this assumption.

In this work, we present the first geochronological constraint, field description and geochronological data of these volcanic rocks. The obtained ages indicate that this volcanic episode took place, indeed, during the middle to late Miocene, briefly coeval to postdating compressive tectonics recognized through the fold and thrust belt (Bechis et al., 2014; Bilmes et al., 2013; Orts et al., 2012). Additionally, these sections show a synextensional character evidenced by the depocenter architecture and the structural analysis. Geochronological determinations indicate that these sections have accumulated coevally with the last phase of pluton emplacement of the North Patagonian Batholith (Pankhurst et al., 1999). Geochemical data were used to compare these occurrences, east of the arc front, with coetaneous arc and back-arc products through the area.

This study provides new insights about the late Cenozoic tectonics of a poorly known segment of the Andes, which indicate the existence of an extensional phase that affected the inner sector of the fold and thrust belt during and after the main contractional stage. This study case may contribute to a general discussion about the mechanisms that eventually could trigger extension in the hinterlands of a subduction-related mountain system.

http://dx.doi.org/10.1016/j.tecto.2015.06.032
0040-1951/

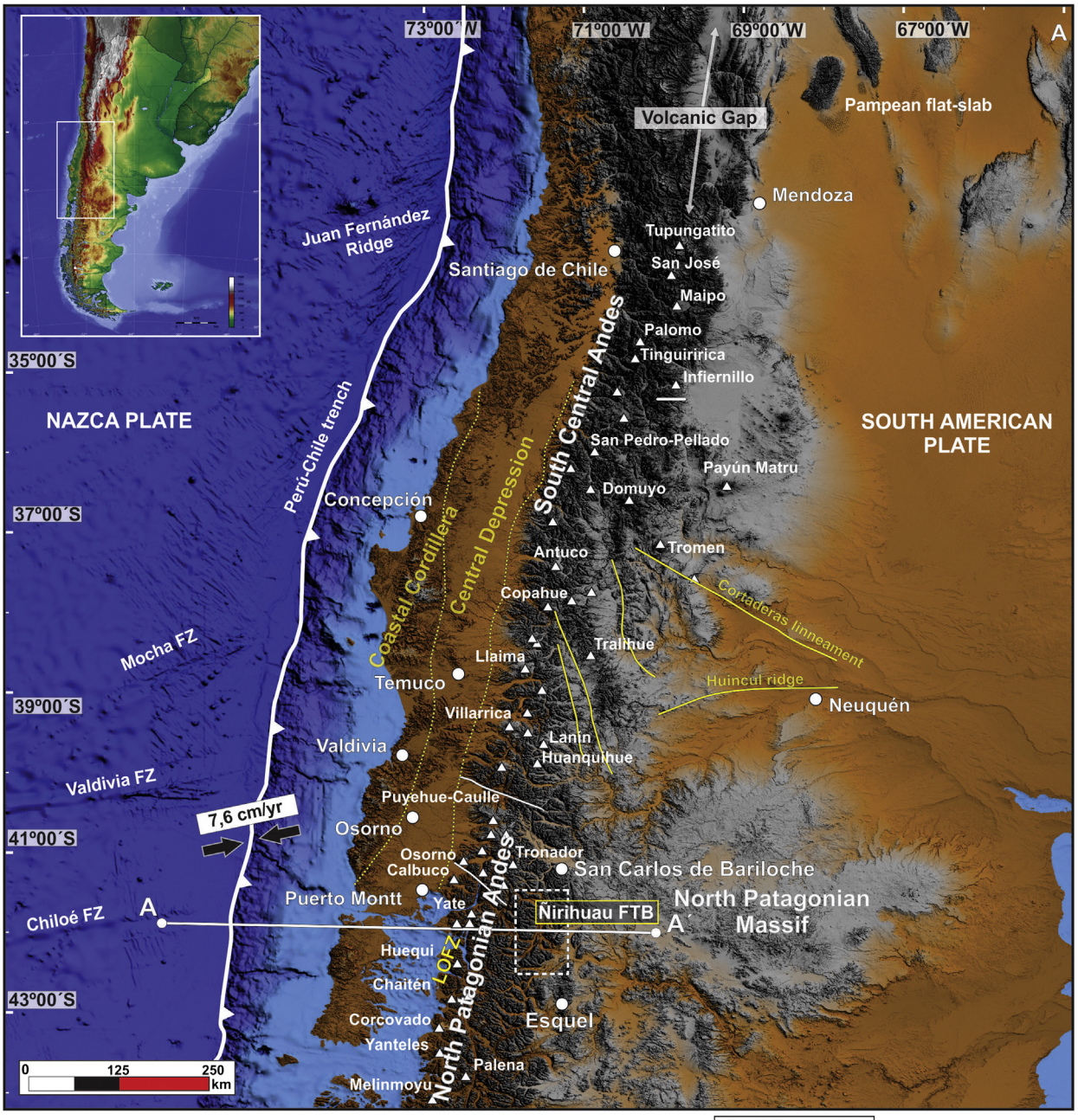

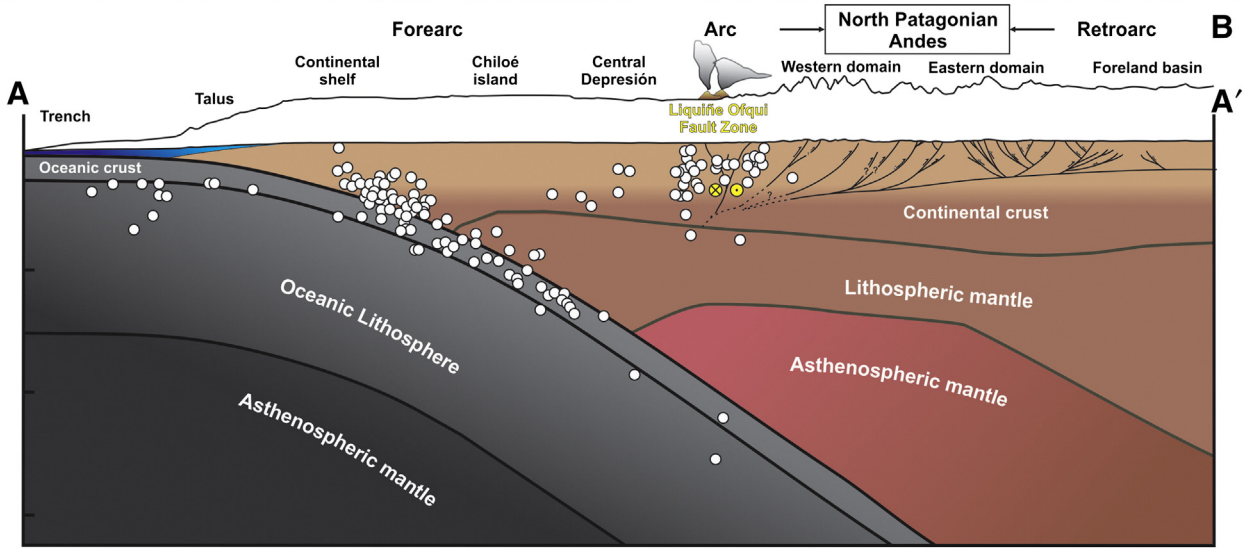

Please cite this article as: Tobal, J.E., et al., Middle to late Miocene extensional collapse of the North Patagonian Andes (41°30′–42°S), Tectonophysics (2015), http://dx.doi.org/10.1016/j.tecto.2015.06.032

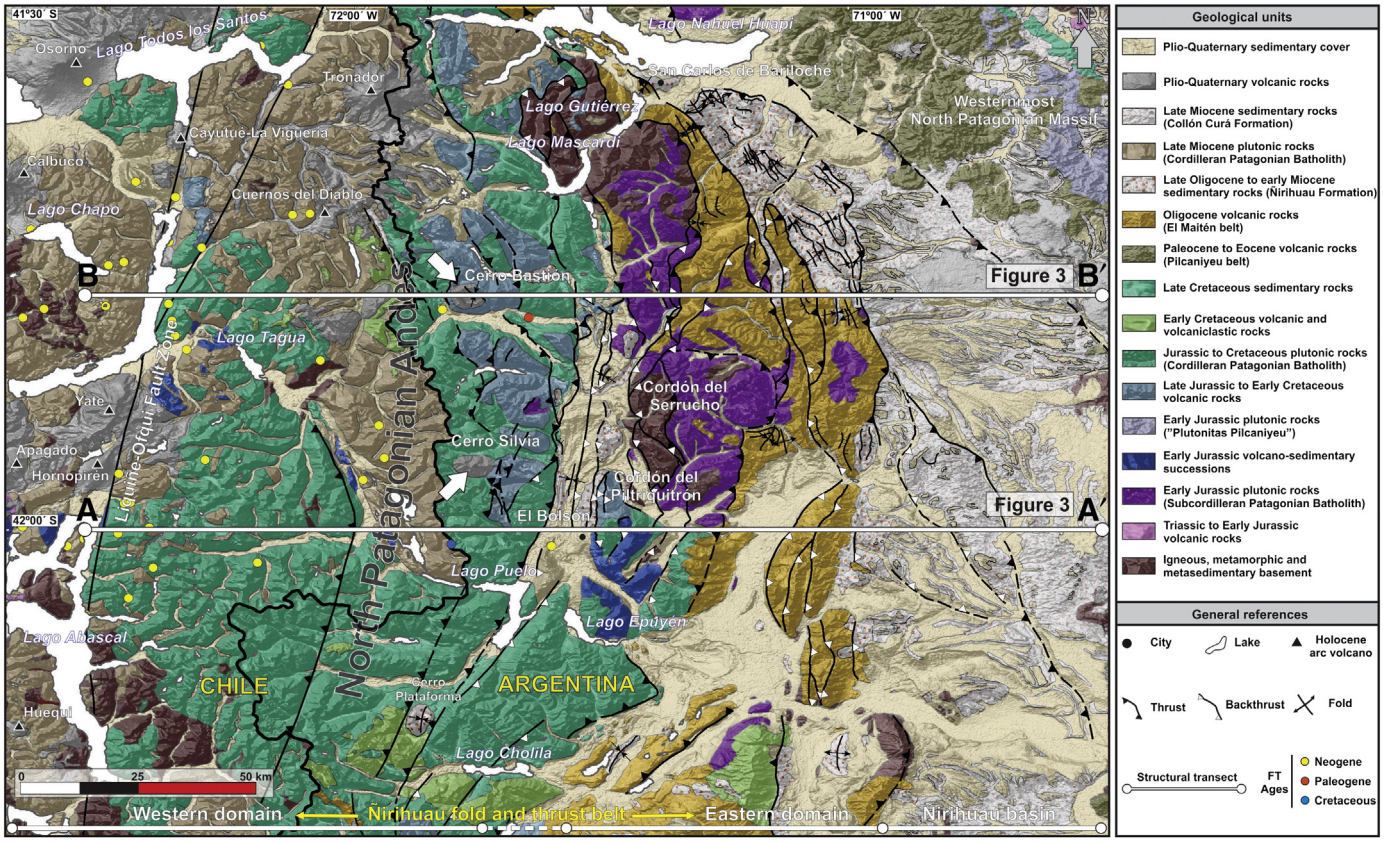

Fig. 2. Geological map of the North Patagonian Andes between 41° and 43°S (data compiled from Adriasola et al., 2006; Duhart et al., 2000; Diez and Zubia, 1981; Giacosa et al., 2001; Lizuaín and Viera, 2010; and our own data). White arrows indicate Cerro Bastión and Cerro Silvia areas, where this study is focused. Note that late Pleistocene to Holocene volcanoes (black triangles) are aligned with the Liquiñe–Ofqui fault zone (LOFZ), and that the fold and thrust belt presents a characteristic curved shape with a convexity towards the foreland.

2. Geological framework of the North Patagonian Andes

The North Patagonian Andes extend from 39° to 46°S constituting a relatively low mountain range (Fig. 1A), with a steep relief affected by Plio-Pleistocene glacial erosion. This Andean segment developed during the last ~110 Ma by the continuous subduction of a series of oceanic plates beneath the South American plate (Maloney et al., 2013). At the end of the Oligocene, a major change in the direction of convergence associated with the breakup of the Farallon plate occurred (Lonsdale, 2005; Somoza and Ghidella, 2012). The newly formed Nazca plate began to subduct in a trench-orthogonal direction and the rate of convergence between Nazca and South America plates incremented during early Miocene times (Somoza and Ghidella, 2012), which led to an event of mountain building along the Central and Patagonian Andes. The Nazca plate is now subducting in this region at a normal dip (~30°) along the Chilean trench, north of the Chilean Triple Junction that separates this plate from the Antarctic and South American Plates to the south (Lange et al., 2008; Fig. 1B).

2.1. Lithotectonic domains

Three lithotectonic domains are differentiated from west to east, over the eastern Andean slope between 40° and 43°S (Figs. 1B and 2):

1) A western domain of the North Patagonian Andes, where the 2000 km long, 200 km wide north-south Patagonian Batholith is the most outstanding feature; this comprises calc-alkaline plutonic rocks of Middle Jurassic to Miocene age (Pankhurst et al., 1999; Hervé et al., 2007, and references therein).
2) An eastern domain of the North Patagonian Andes, where a late Paleozoic basement (Dalla Salda et al., 1991; González Bonorino, 1944) and the Early Jurassic Subcordilleran Patagonian Batholith (Gordon and Ort, 1993) are unconformably covered by the Oligocene El Maitén volcanic belt (Rapela et al., 1988).
3) The Ñirihuau foreland basin infill, conformed by fluvial, lacustrine and pyroclastic deposits of late Oligocene to late Miocene age (Cazau et al., 1989; Mancini and Serna, 1989; Mazzoni and Benvenuto, 1990; Paredes et al., 2009), which covers part of the eastern flank of the North Patagonian Andes and is limited to the east by the North Patagonian Massif.

In addition, the Liquiñe Ofqui fault zone (Cembrano et al., 1996; Hervé, 1976), located west of the main Andes, is one of the longest active strike-slip fault systems (more than 1000 km long) in modern subduction settings (e.g. Jarrard, 1986). This long-term regional-scale structure controlled the emplacement of Miocene plutons along the axis of the cordillera (Adriasola et al., 2006; Thomson, 2002) and concentrated late Pleistocene and Holocene arc volcanic activity (Lavenu and Cembrano, 1999). Crustal seismic activity at these latitudes and associated neotectonic deformation are limited to this sector (Lange et al., 2008; Vargas et al., 2013).

Fig. 1. A) Present tectonic setting of the South Central and North Patagonian Andes, showing the interaction between South American and Nazca plates. Black arrows indicate the direction and the average convergence rate for the last 5 Ma (Somoza and Ghidella, 2012). White triangles represent the location of arc-volcanoes with late Pleistocene to Holocene activity (after Siebert and Simkin, 2002). White box indicates the study area represented in Fig. 2. FZ: Fracture zone. FTB: Fold and thrust belt. The base map was constructed superposing a slope map over a hill shade map using topographic data from http://www.gdem.aster.ersdac.or.jp/index.jsp; B) Crustal cross section at 42°S (modified from Orts et al., 2012) and upper crustal structures of this work (seismicity is after Lange et al., 2008).

Please cite this article as: Tobal, J.E., et al., Middle to late Miocene extensional collapse of the North Patagonian Andes (41°30′–42°S), Tectonophysics (2015), http://dx.doi.org/10.1016/j.tecto.2015.06.032

2.2. Main geological units

An upper Paleozoic metamorphic basement is exposed both at the Chilean coast and at the eastern domain of the North Patagonian Andes. The basement, over the eastern Andean slope, comprises late Paleozoic metamorphic rocks between Lago Nahuel Huapi (~41°S) and Lago Cholila (~42° 30′ S) (Dalla Salda et al., 1991; González Bonorino, 1944). Schists, gneisses, metaquartzites, amphibolites and migmatites intruded by syn- to post-tectonic granitoids crop out in the vicinities of Mascardi and Gutiérrez lakes, in the Cordón del Serrucho and in the Cordón del Piltriquitrón (González Bonorino, 1944; Dalla Salda et al., 1991; Giacosa et al., 2001; García-Sansegundo et al., 2009; Fig. 2). Pankhurst et al. (2006) reported U–Pb SHRIMP Early Carboniferous ages of 323 ± 3, 330 ± 4 and 329 ± 4 Ma for these rocks, confirming a conventional U–Pb zircon age of 321 ± 2 Ma, previously reported by Varela et al. (2005). Mostly igneous Late Triassic to Lower Cretaceous units cover and intrude the basement rocks through northwestern Patagonia from the main Andes to the foreland. Early Jurassic intrusives (184–181 Ma; Gordon and Ort, 1993; Rapela et al., 2005) are exposed in the eastern domain of the North Patagonian Andes between 41° and 43°S. These form a NNW-trending Subcordilleran Patagonian Batholith (SPB) that extends for more than 250 km, further south of the study area.

Middle Jurassic to Upper Cretaceous calc-alkaline granitoids of the Cordilleran Patagonian Batholith (CPB) crop out as the dominant rocks along the highest part of the Andes from San Carlos de Bariloche (~41°S) to Esquel (~43°S) (Castro et al., 2011; Diez and Zubia, 1981; Giacosa et al., 2001; Lizuaín and Viera, 2010; SERNAGEOMIN-BRGM, 1995). Recent U–Pb SHRIMP age determinations indicate a Middle to Late Jurassic age for these tonalites and granodiorites (and to a lesser extent, granitic porphyries). K–Ar and Rb-Sr geochronology span from Middle Jurassic times, as old as ca. 170 Ma (Halpern et al., 1975), to the Cretaceous ~71 Ma (González Díaz, 1982; González Díaz and Valvano, 1978; Lizuaín, 1980).

In addition, the western domain of the North Patagonian Andes exhibits a complex and poorly outlined interplay of sedimentary and volcanic sequences of Early Jurassic–Lower Cretaceous age (Diez and Zubia, 1981; Giacosa et al., 2001; González Bonorino, 1944, 1974; González Díaz, 1982; González Díaz and Lizuaín, 1984; Lizuaín, 1980, 1981; Thiele et al., 1978). Early Jurassic volcano-sedimentary sections were identified in the Cordón del Piltriquitrón and also occur as very small, isolated outcrops at the highest parts of the Andes (González Bonorino, 1944, 1974; Lizuaín, 1980; Lizuaín and Viera, 2010; Fig. 2). These rocks are covered by Middle to Late Jurassic volcanic rocks, mainly andesites with subordinate dacites (Diez and Zubia, 1981; Giacosa et al., 2001; Tobal et al., 2012) and late Early Cretaceous volcanic rocks (Aragón et al., 2012; De La Cruz et al., 2003; Lizuaín and Viera, 2010; Pankhurst et al., 2003; Suárez et al., 1996). These volcanic units, continuously exposed through the Andean front, are barely distinguishable in the field (Giacosa et al., 2001), so they are described here as a single unit (Fig. 2).

Two well-defined volcanic belts of Paleogene age are represented in the study area at the foreland and the eastern domain of the North Patagonian Andes respectively (Rapela et al., 1988): i) an eastern latest Cretaceous–Eocene belt (60 to 42 Ma; Rapela et al., 1983), the Pilcaniyeu belt, which encompasses bimodal calc-alkaline volcanic rocks (basalt–rhyolite) with large amounts of ignimbrites and subordinate andesites and basalts towards the top of the sequence (Rapela et al., 1988); and ii) a western Oligocene–lower Miocene belt (33–21 Ma; Cazau et al., 1989), the El Maitén belt, which consists of thick piles of andesites and dacites with lesser amounts of rhyolites and basalts (González Bonorino, 1973; González Bonorino and González Bonorino, 1978; Rapela et al., 1988).

During Neogene times, fluvial and deep lacustrine sediments of the Ñirihuau Formation (González Bonorino, 1973) and fluvial, lacustrine and eolian deposits of the Collón Curá Formation (Feruglio, 1947; González Bonorino, 1944; Mazzoni and Benvenuto, 1990; Yrigoyen, 1969), filled the Ñirihuau basin. Coevally, late Miocene plutons of the North Patagonian Batholith were coevally emplaced to the west, mainly over the Chilean territory (Aragón et al., 2012; González Díaz, 1979, 1982; González Díaz and Valvano, 1978; Pankhurst et al., 1999; Rapela et al., 1987; Sernageomin-BRGM, 1995).

In Pliocene to Quaternary times, basaltic–andesitic flows were emplaced in both the foreland area, as within plate eruptions (Massaferro et al., 2006; Pécskay et al., 2007), and on the western slope of the main Andes, as arc-related rocks (see Lara et al., 2001, and references therein). The thickest succession of these volcanic rocks is present at the Tronador volcanic center as part of the arc front at the international boundary between Argentina and Chile (Rabassa et al., 1986).

2.3. The Ñirihuau fold and thrust belt

In the North Patagonian Andes, between 41° and 43°S, the Ñirihuau fold and thrust belt develops east of the Liquiñe Ofqui Fault Zone (Ramos and Cortés, 1984; Giacosa and Heredia, 2004; Figs. 1B and 3). This deformational belt presents a convex-to-the-foreland shape in map view with two distinguishable domains: i) a western domain at the hinterland, characterized by basement-involved faults affecting at surface mainly igneous Mesozoic units; and ii) an eastern domain, which includes Oligocene volcanic rocks of the El Maitén belt and Neogene synorogenic deposits deposited in the wedge top and the foreland zones with predominant thin-skinned deformation (Ramos and Cortés, 1984; Giacosa and Heredia, 200; Bechis and Cristallini, 2006).

The Bolsón–Tronador thrust that uplifts the eastern flank of the western domain of the North Patagonian Andes and the Serrucho–Piltriquitrón back-thrust system in the western slope of the eastern domain define a triangular zone that characterizes the El Bolsón valley. This narrow topographic depression constitutes a sub-basin presently disconnected from the main Ñirihuau basin developed at the foreland (Bechis et al., 2014; Fig. 3).

Main N- to NW-trending thrusts developed through both the hinterland and the foreland zones detached from two décollements interpreted from seismic data at the foreland (Bechis and Cristallini, 2006; Orts et al., 2012; Fig. 3). To the west, Tobal et al. (2012) described a cannibalized thin-skinned fold and thrust belt affecting the Late Jurassic to Early Cretaceous volcanic rocks exposed in the Cordón del Hielo Azul (Fig. 3).

3. Cenozoic volcanic rocks at the inner sector of North Patagonian fold and thrust belt

Three isolated volcanic successions hosted at the North Patagonian Andes between 41° and 42° 30′ S have been previously attributed to the Oligocene Ventana Formation (Diez and Zubia, 1981; Giacosa et al., 2001; Lizuaín and Viera, 2010; Sepúlveda and Viera, 1980; Tobal et al., 2012). These are the Cerro Bastión and Cerro Silvia represented in Fig. 2, and Cordón del Ingeniero located immediately to the south. Volcanic rocks composed of andesitic to basaltic agglomerates, tuffs and lava flows lying unconformably over Mesozoic strata were analyzed in the Cerro Bastión and Cerro Silvia (Fig. 2). Field, petrographic, geochronological and geochemical data show the emplacement, timing and their tectonic setting in the Cerro Bastión and Cerro Silvia rocks.

3.1. Description of the volcanic units

3.1.1. Cerro Silvia area

The Cerro Silvia is part of the Cordón del Hielo Azul, a range located west of the El Bolsón village, between 41° 50′ and 42° 00′ S, bounded to the north by the Azul river and to the south by the Blanco del Motoco creek (Fig. 4). This N-trending range comprises a deformed belt of Late Jurassic to Early Cretaceous volcanic rocks (González Díaz, 1982).

Please cite this article as: Tobal, J.E., et al., Middle to late Miocene extensional collapse of the North Patagonian Andes (41°30′–42°S), Tectonophysics (2015), http://dx.doi.org/10.1016/j.tecto.2015.06.032

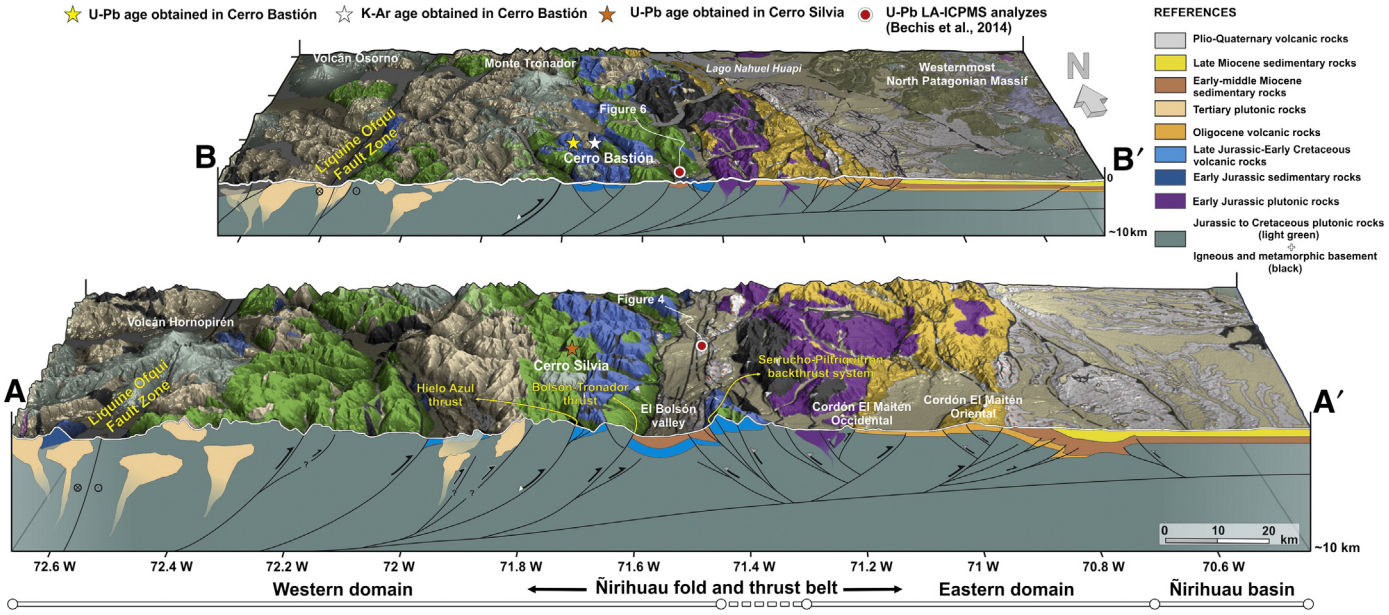

Fig. 3. Three-dimensional (3D) block diagrams showing regional structural cross-sections of the Ñirihuau fold and thrust belt together with digital elevation models and geological information on top of them (after Giacosa and Heredia, 2004; Bechis and Cristallini, 2006; Orts et al., 2012). Stars represent the location of the K–Ar and U–Pb samples obtained in this work. Red-white dots indicate the U–Pb LA-ICPMS analyses of the Ñirihuau formation (data from Bechis et al., 2014). Colors used in references apply to the units of the cross-sectional profiles (at depth) rather than colors of the 3D view of the geology (at surface), which are somewhat different because of the texture that imposes the relief. Basement rocks and Mesozoic plutonic bodies of the North Patagonian Batholith are represented as a whole at depth despite its discrimination at surface (light green vs. black color). (For interpretation of the references to color in this figure legend, the reader is referred to the web version of this article.)

Cretaceous granitoids of the N-trending Cordilleran Patagonian Batholith are intruding the Cretaceous volcanic rocks (Fig. 4). The westernmost recognized structure (*Hielo Azul thrust*; Giacosa et al., 2001) corresponds to a reverse fault that defines one of the main topographic breaks at these latitudes (Tobal et al., 2012). Locally, at the Cerro Silvia area, the hanging wall of this structure is topographically depressed with respect to neighbor regions (Fig. 4). The volcanic rocks outcropping throughout this range were previously assigned to the El Maitén belt (Diez and Zubia, 1981; Giacosa et al., 2001). The internal arrangement of these volcanic rocks shows a wedge-like geometry formed by progressive unconformities that widen to the east, against the west-dipping fault that affected Late Jurassic to Early Cretaceous volcanic rocks on the footwall (Fig. 5). Since the age determination performed in this study indicates a younger, middle Miocene age for these rocks (see Section 3.2), we interpret that this thrust was reactivated as a normal fault during middle Miocene times.

The Cerro Silvia volcanic succession includes dacitic pyroclastic rocks, andesitic lava flows and a small dioritic pluton. The pyroclastic sections are dominant and include matrix-supported lithic and vitric tuffs. They consist of devitrified pumice fragments, volcanic lithic clasts and plagioclase, K-feldspar and embayed quartz crystal fragments. The matrix comprises fine ash vitric particles and minor small crystal

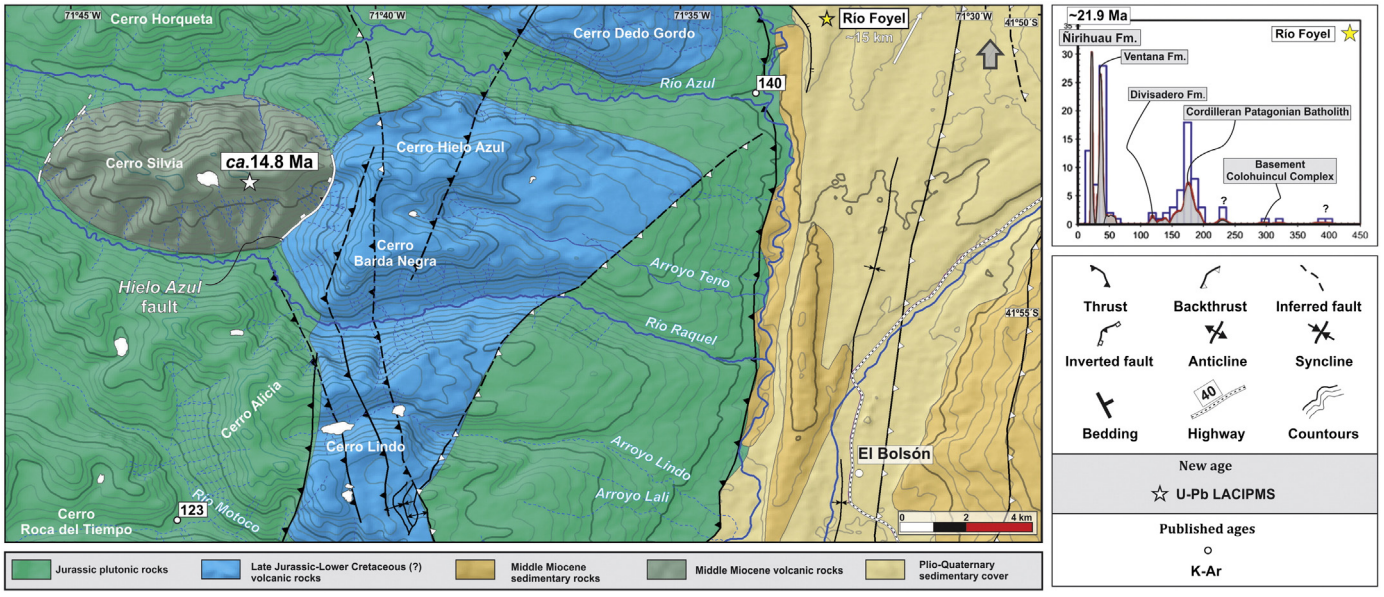

Fig. 4. Geological map of the Cerro Silvia area, in the western domain of the Ñirihuau fold and thrust belt, between 41°50′ and 42°′ S (modified after Diez and Zubia, 1981; Giacosa et al., 2001; Tobal et al., 2012; Bechis et al., 2014). N-trending thrusts and backthrusts affect the Mesozoic volcanic rocks defining thin- and thick-skinned deformational zones (Tobal et al., 2012). Middle Miocene volcanic rocks (white star indicate the new U–Pb LACIPMS age) crop out in the Cerro Silvia at the hanging-wall of an innermost thrust sheet.

Please cite this article as: Tobal, J.E., et al., Middle to late Miocene extensional collapse of the North Patagonian Andes (41°30′–42°S), Tectonophysics (2015), http://dx.doi.org/10.1016/j.tecto.2015.06.032

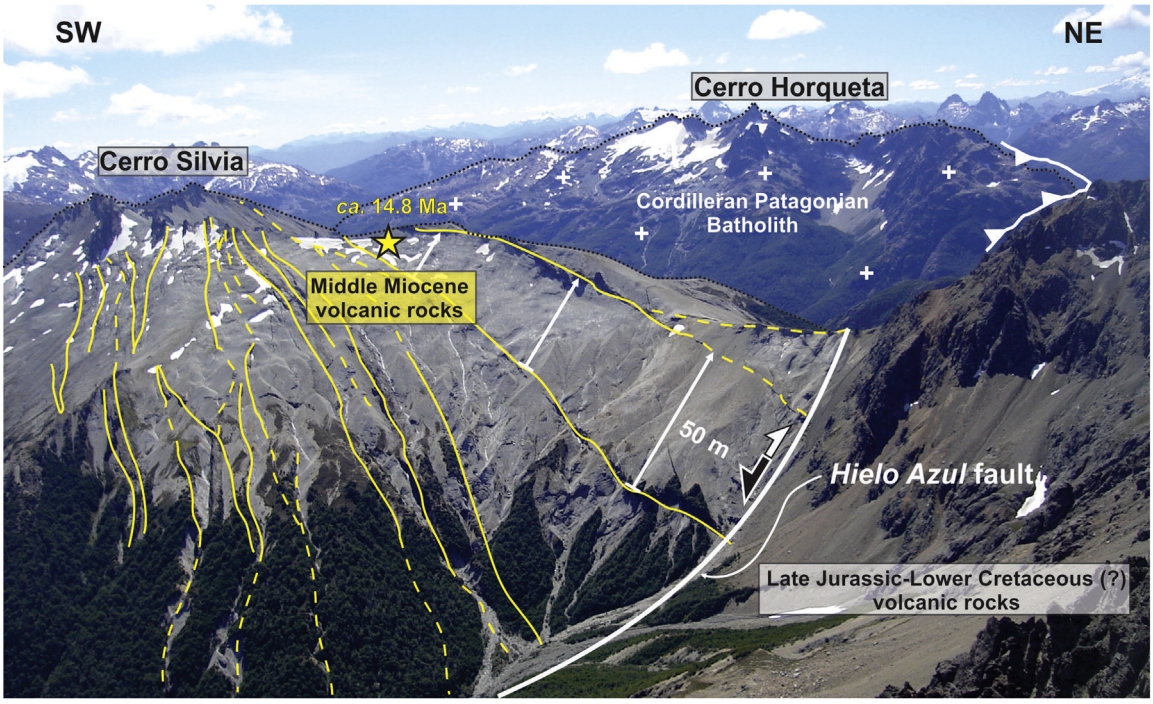

Fig. 5. The *Hielo Azul thrust* (Giacosa et al., 2001) would have been reactivated as a normal fault that controlled the infill of the middle Miocene volcanic rocks in the Cerro Silvia. These volcanic and pyroclastic rocks were emplaced in the hanging wall of the fault, superposed to Mesozoic volcanic rocks that also outcrop to the east, in the footwall of the fault. Middle-Upper Jurassic plutonic rocks of the Cordilleran Patagonian Batholith limit this volcanic depocenter to the north and south (outside the picture; see Fig. 4).

fragments. Intercalated andesitic lava flows are composed of plagioclase, amphibole and opaque minerals phenocrysts in a hyalopilitic, felty or microgranophyric groundmass. A sample from a lava flow was dated by U–Pb LA-CIPMS method in zircons (see Section 3.2).

3.1.2. Cerro Bastión area

The Cerro Bastión area, located between 41° 30′ and 41° 35′ S, is bounded to the north by the Martin and Steffen lakes and to the south by the Manso Inferior river (Fig. 6). This originates in Lago Steffen, flowing to the south and then changing abruptly its flow to the west into Chilean territory along a wide and flat valley. Both the Cerro Bastión and Cerro Santa Helena define an L-shaped hill with an abrupt relief covered by extensive vegetation in the lower slopes (Fig. 6).

At the eastern flank of the range, plutonic rocks of the Cordilleran Patagonian Batholith crop out in the Cerro Santa Helena (Diez and Zubia, 1981; Giacosa et al., 2001). A previous Rb–Sr whole-rock isochron age of 170 Ma (Halpern et al., 1975) resulted concordant with Middle-Jurassic (168.9 to 154.5 Ma) U–Pb SHRIMP ages recently obtained by

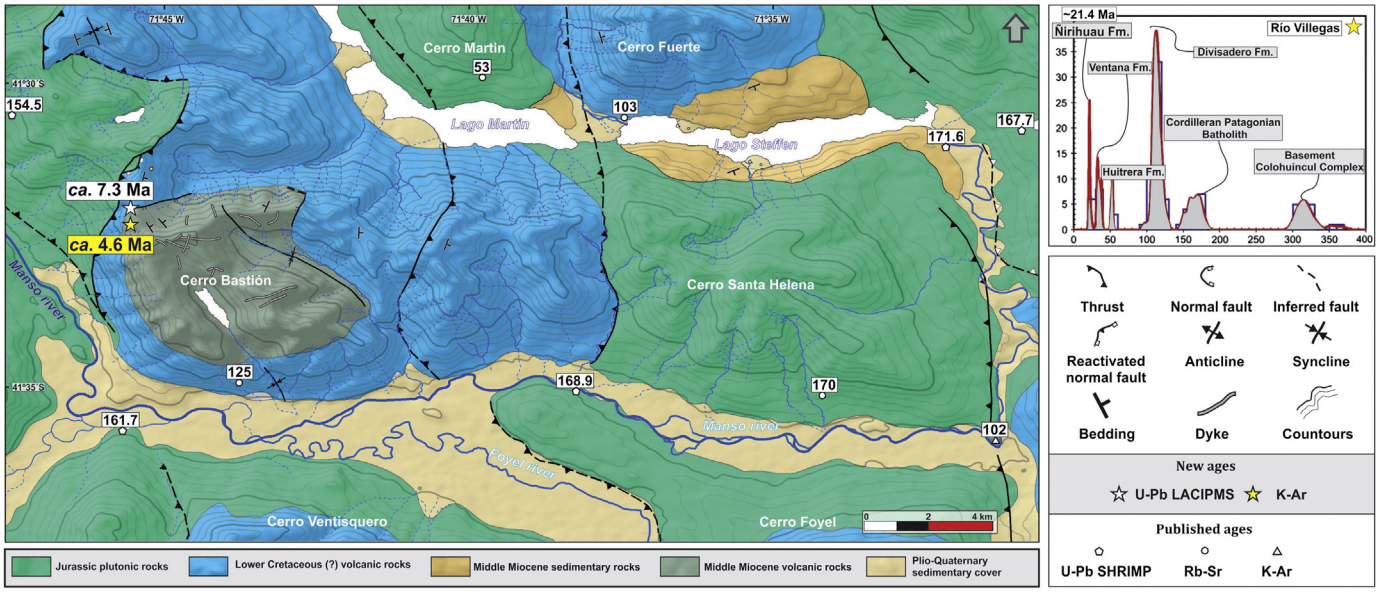

Fig. 6. Geological map of the Cerro Bastión area, in the western domain of the Ñirihuau fold and thrust belt, between 41°29′ and 41°38′ S (modified after Diez and Zubia, 1981; Giacosa et al., 2001). E- to ESE-trending thrusts structure this Andean segment together with main N-trending thrusts that characterize the Ñirihuau fold and thrust belt. In the Cerro Bastión, Miocene volcanic rocks are unconformably overlain Mesozoic rocks. White and yellow stars indicate new U–Pb (LAICPMS) and K–Ar ages respectively obtained in the Cerro Bastión volcanic rocks in this work.

Please cite this article as: Tobal, J.E., et al., Middle to late Miocene extensional collapse of the North Patagonian Andes (41°30′–42°S), Tectonophysics (2015), http://dx.doi.org/10.1016/j.tecto.2015.06.032

Castro et al. (2011) (Fig. 6). To the west and the northeast, volcanic rocks assigned to the Upper Jurassic-Lower Cretaceous interval unconformably cover the Jurassic plutonic rocks (Diez and Zubia, 1981). The early Miocene Río Villegas synorogenic clastic succession, deposited on top of these volcanic rocks, in the westernmost El Bolsón valley, shows a maximum detrital peak at ~113 Ma. This age indicates the presence of volcanic rocks of the Divisadero Formation, constraining the age of the Mesozoic volcanic rocks to the Cretaceous (see Bechis et al., 2014, Fig. 9C). Detrital zircon pattern also records the exhumation of the Middle to Late Jurassic granitoids of the Cerro Santa Elena area to the west. Another source area is seen with zircon peaks derived from late Paleozoic basement and the Oligocene Ventana Formation cropping out immediately to the east (Bechis et al., 2014).

Early Miocene sedimentary rocks of the Ñirihuau Formation crop out at both margins of Lago Steffen and in the Río Villegas areas (Giacosa et al., 2001; Fig. 6). A maximum age of ~18.3 Ma is indicated by the U–Pb from detrital zircons (Bechis et al., 2014).

Lighter-colored-volcanic rocks cropping out at the highest parts of the Cerro Bastión unconformably overlay lavas and breccias of the Late Jurassic to Early Cretaceous volcanic rocks (Fig. 7). The volcanic succession at Cerro Bastión has a minimum thickness estimated in ~280 m. As in the Silvia area, dacitic ignimbrite packages alternate with andesitic lava flows with subordinate pyroclastic surges and ash fall deposits at the uppermost levels (Fig. 7). Pyroclastic rocks comprise lithic and vitric tuffs while andesitic lava flows usually exhibit porphyritic textures with plagioclase, hornblende, and minor clinopyroxene and opaque minerals.

Normal faults that juxtapose Cenozoic strata to Lower Cretaceous sections controlled eastern and northwestern edges of the depocenter that hosts these volcanic successions (Fig. 8). Even though these rocks were previously assigned to the Oligocene Ventana Formation (Diez and Zubia, 1981; Giacosa et al., 2001), two samples dated by U–Pb and K–Ar methods have yielded considerably younger ages. A lava flow at the mid part of the volcanic succession was dated by the K–Ar method, while a pyroclastic rock located below was analyzed by the U–Pb LACIPMS method (see next section).

3.2. Geochronology

Two volcanic rocks from the Cerro Silvia (SIL-1) and Cerro Bastion (BSMU-2) were selected for U–Pb analysis (see Figs. 4 and 6 for their location). The zircon grains were separated from approximately 5 kg of samples from an andesite (SIL-1) and a pyroclastic rock (BSMU-02). Heavy mineral fractions were concentrated and separated into 100, 150 and 250 μm size fractions by standard crushing and panning at the Universidad de Buenos Aires. Zircon fractions of roughly 400 grains were handpicked in alcohol under a binocular microscope for geochronological analysis. The zircon U–Pb analyses were made using the Micromass Isoprobe Multicollector ICPMS at the Washington State University. Sample coordinates, analytical methods, and U–Pb

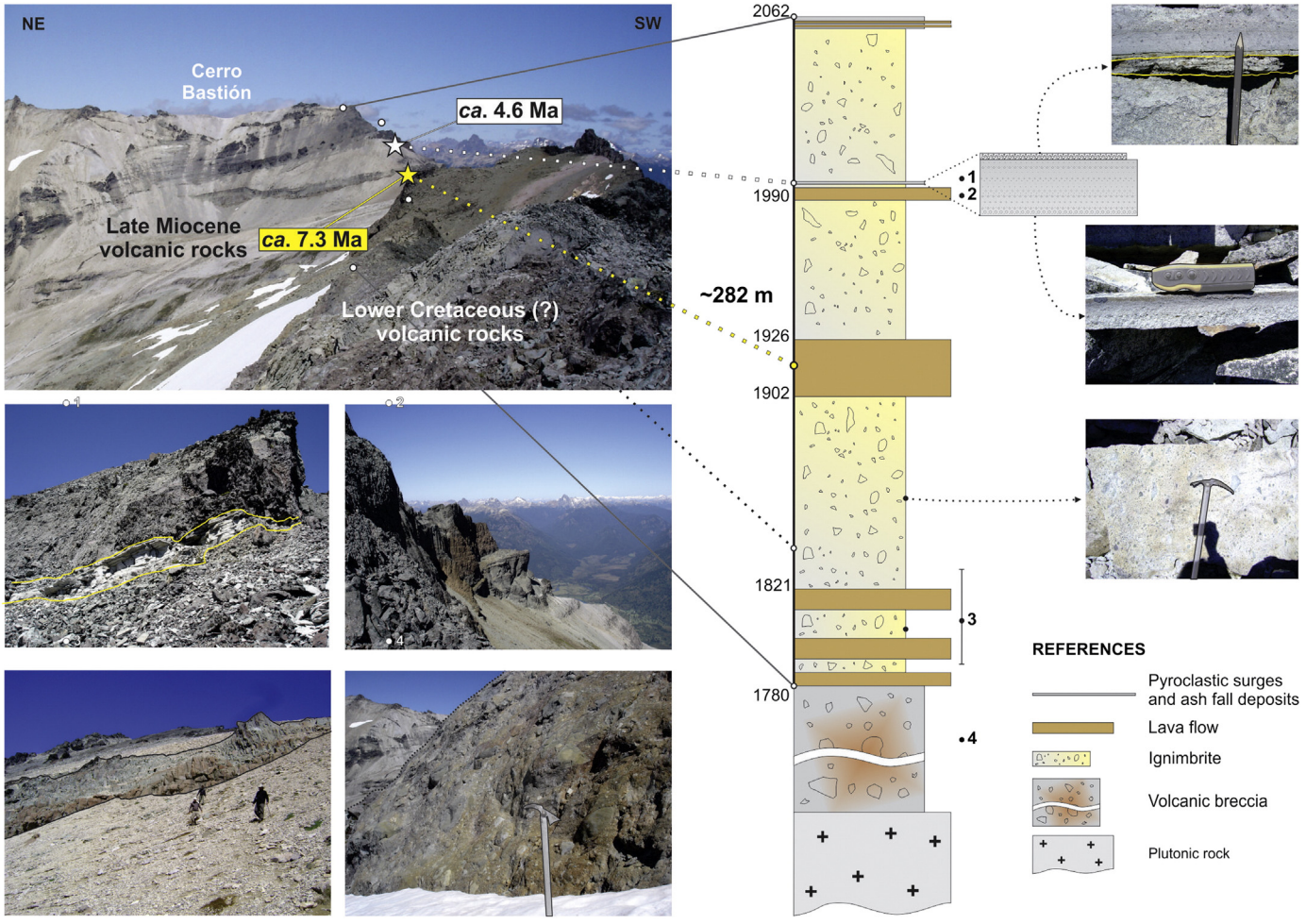

Fig. 7. Volcanic succession at Cerro Bastión. Upper left picture shows the development of the volcanic section. Thick packages of ignimbrites alternate with lava flows of variable thicknesses through the section that at the top are intercalated with subordinated pyroclastic surges and ash fall deposits. The entire volcanic pile lies in fault contact upon volcanic breccias of the Divisadero Formation. Intrusive rocks of the Cordilleran Patagonian Batholith constitute the basement of the section. Pictures of representative different levels are also displayed indicating their location in the profile.

Please cite this article as: Tobal, J.E., et al., Middle to late Miocene extensional collapse of the North Patagonian Andes (41°30′–42°S), Tectonophysics (2015), http://dx.doi.org/10.1016/j.tecto.2015.06.032

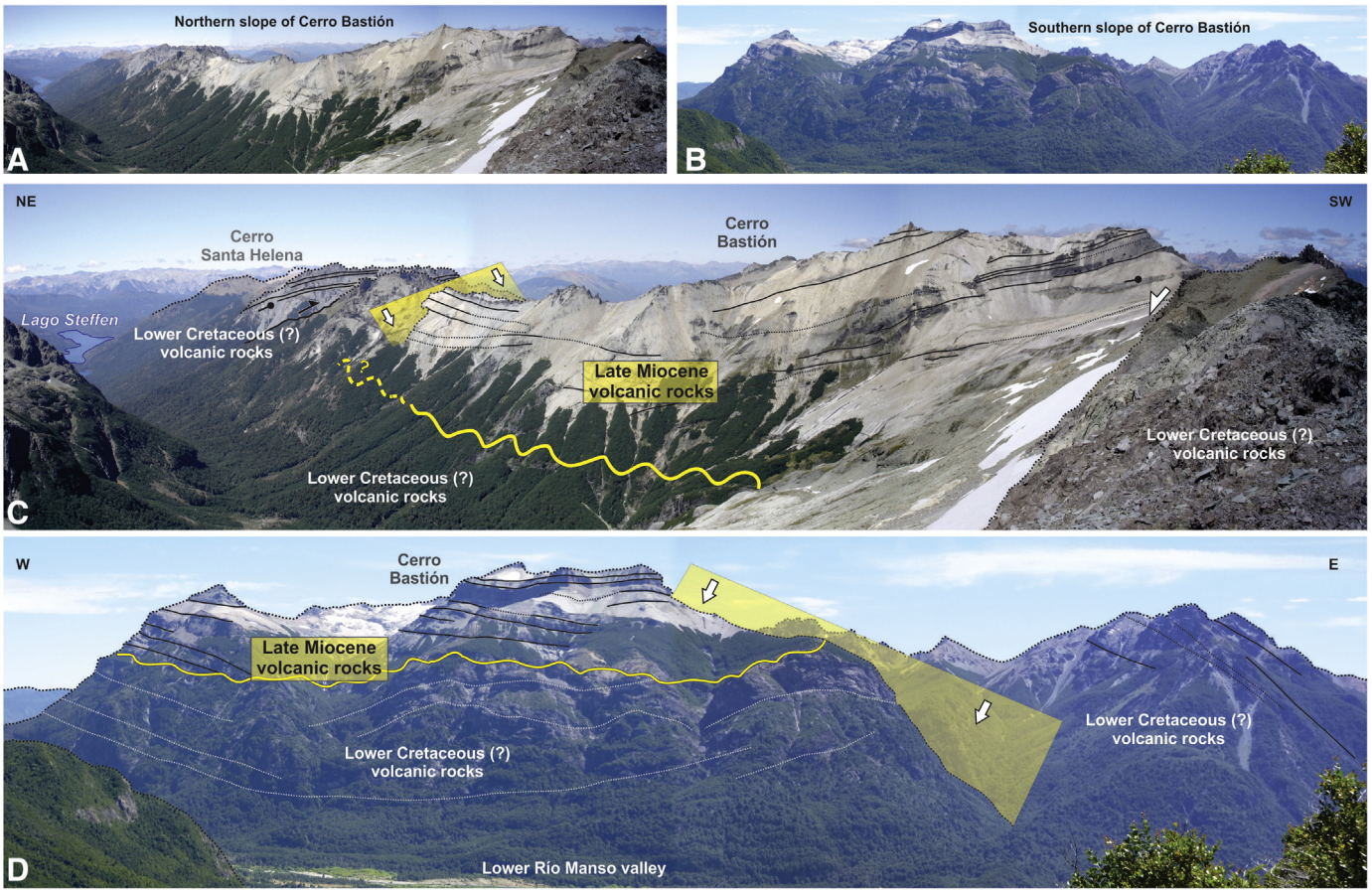

Fig. 8. Panoramic views of the late Miocene–early Pliocene volcanic rocks of the Cerro Bastión. These rocks, unconformably overlie and are in fault contact with Aptian volcanic rocks of the Divisadero Formation, constituting a volcanic depocenter controlled by normal faults (indicated by white arrows). To the east (left side of the diagram), there is a thrust affecting Mesozoic volcanic rocks that outcrop in the easternmost part of the Cerro Bastion and the adjacent Cerro Santa Helena.

age measurements of zircon grains are available in the Supplementary Material (Appendix A and B). Approximately 30 m above the BSMU-2 sample (see Fig. 7), an andesitic lava flow (sample 9) was dated by K–Ar (whole rock analysis performed by SERNAGEOMIN, Chile; see table with K–Ar values in the Supplementary Material; Appendix B).

One hundred zircons from the sample SIL-1 (Cerro Silva) were mounted, from which 40 grains were analyzed. Among these, 32 analyzes produced a main peak at ca. 14.8 Ma which is according to the tuff zircon age calculated by isoplot at 14.8 + 0.7/−0.3 Ma. The remaining 8 grains are represented by single ages at ca. 21, 32, 33, 39, 160, 262, 264, and 323 Ma (Fig. 9a). Tera–Wasserburg diagram is shown in Fig. 9b. Elongate prismatic crystals are observed with oscillatory zoning textures in the cathodoluminescence image, indicating a volcanic origin for the analyzed zircons (Fig. 9c). The crystallization age of the Cerro Silvia andesite is ca. 14.8 Ma.

In sample BSMU-2 (Cerro Bastion), 100 zircons were mounted and 39 grains were analyzed by U–Pb. The data define a main peak at ca. 7.2 Ma (ages between 7.0 Ma and 9.9 Ma), where a single grain has ca. 16.3 Ma. Therefore, the tuff zircon age calculated by isoplot at 7.3 + 0.2/−0.1 Ma corresponds to the main peak (Fig. 9d) (Tera–Wasserburg diagram of the data obtained in this sample is shown in Fig. 9e). The observed zircons have long prismatic habits and idiomorphic forms. In the cathodoluminescence image, the zircon crystals display typically magmatic textures characterized by oscillatory zoning (Fig. 9f), indicating a primary volcanic origin. The crystallization age of this rock is ca. 7.2 Ma. The K–Ar age obtained in the Cerro Bastion (sample 9) of 4.6 ± 0.8 Ma, ~2.6 Ma younger than the U–Pb age (7.2 Ma), is interpreted as a cooling age.

3.3. Geochemistry

Two samples from Cerro Silvia and two from Cerro Bastión were analyzed for major and trace elements. Although there are not perfectly fresh samples (LOI contents of between 0.8 and 4.6%), the normalized (volatile-free) major element composition indicates that Cerro Bastión samples are andesitic, and up to dacitic in the case of Cerro Silvia (Fig. 10A). Samples from both locations are of subalkaline character, with Cerro Bastión having higher alkali contents than Cerro Silva. The relatively low alkali content of Silvia and Bastión samples is similar to the range of compositions displayed by Quaternary arc rocks at the same latitudes, whereas backarc volcanics tend to have higher alkali concentrations (Fig. 10A).

The database used for comparison includes analyses from the stratovolcanoes Osorno (López-Escobar et al., 1992; Tagiri et al., 1993), Calbuco (López-Escobar et al., 1995; Sellés and Moreno, 2011), Yate, Hualaihue, Hornopirén, Huequi, and Michinmahuida (López-Escobar et al., 1993; Watt, 2010; Watt et al., 2011). To characterize the backarc volcanic rocks, we use analyses from the Tronador complex (Mella et al., 2005), although in order to complement the database we have also included backarc samples from further north (~38–39°S; Muñoz and Stern, 1988; 1989). In addition, we included analyses of pyroclastic and volcanic rocks of the Mitrauquén Formation exposed at the main Andes between 38° and 39°S (Muñoz, 1988), which exhibit comparable spatio-temporal characteristics with the here studied volcanic rocks (see Section 5.1 for further details).

As with alkalis, Silvia and Bastión samples have low immobile incompatible element (Nb, Zr, Th, REE) concentrations, similar to the

Please cite this article as: Tobal, J.E., et al., Middle to late Miocene extensional collapse of the North Patagonian Andes (41°30′–42°S), Tectonophysics (2015), http://dx.doi.org/10.1016/j.tecto.2015.06.032

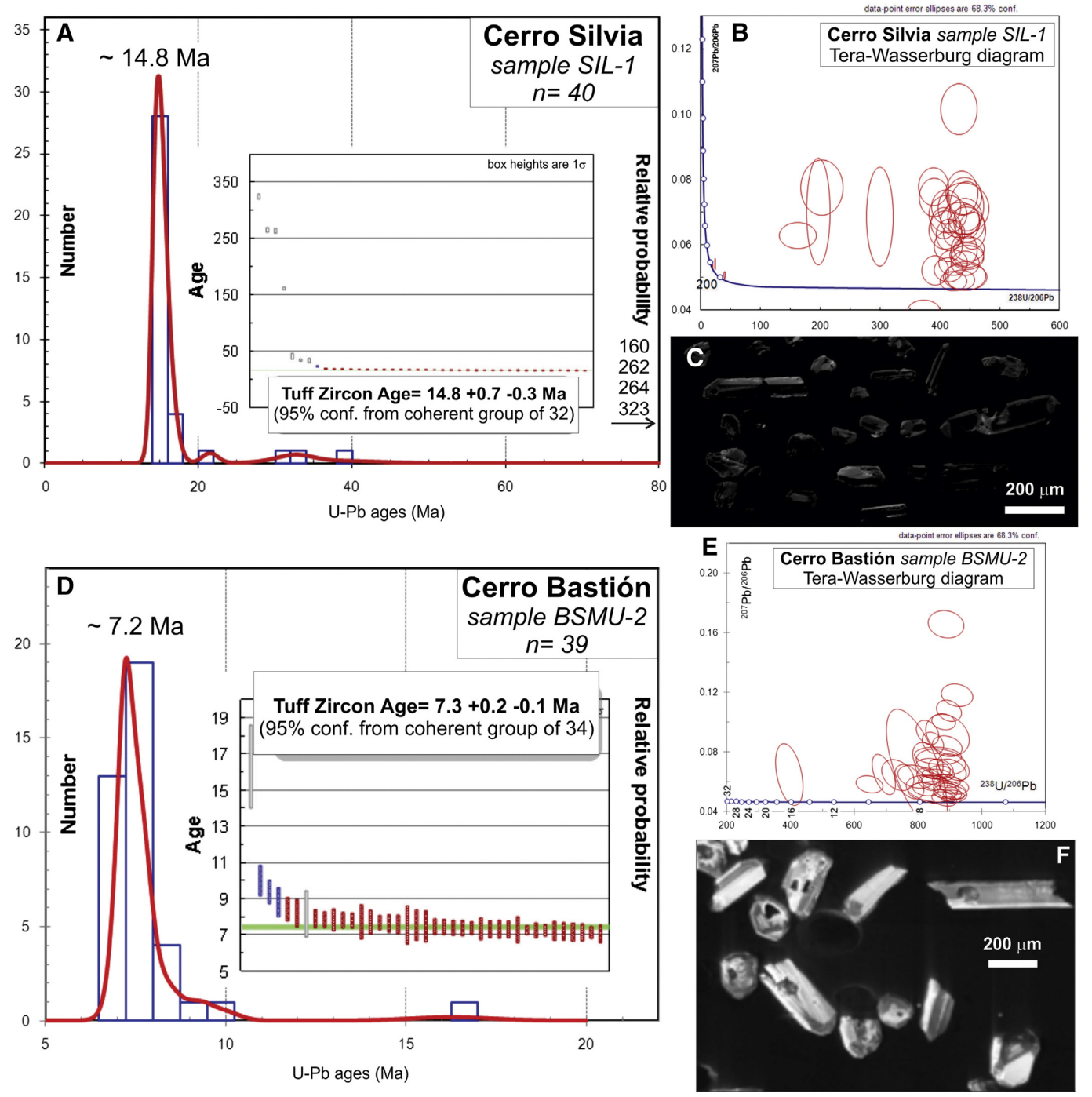

Fig. 9. U–Pb diagrams of the volcanic rocks from the Cerro Silvia and Cerro Bastión; A) frequency histograms and relative probability plots of the sample SIL-1 (inset is the tuff zircon age diagram); B) Tera–Wasserburg concordia diagram of the SIL-1 sample; C) cathodoluminiscence images of some analyzed zircons form SIL-1 sample; D) frequency histograms and relative probability plots of the sample BSMU-2 (inset is the tuff zircon age diagram); E) Tera–Wasserburg concordia diagram of the BSMU-2 sample; and F) cathodoluminiscence images of some analyzed zircons form BSMU-2 sample.

values typical of frontal arc volcanics, whereas backarc volcanoes and volcanic and pyroclastic rocks of the Mitrauquén Formation have higher concentrations (Fig. 10C–D–E). Bastión and Silvia also share with the volcanic front more pronounced low Nb/La and high Ba/La ratios that are characteristic of arc magmatic rocks, although one of the samples (SIL-007) seems to have disturbed Ba concentrations (Fig. 10F–G).

The rare earth element concentrations of Bastión and Silvia are within the range of concentrations displayed by frontal arc rocks with similar silica content ($55 < SiO_2 < 70$), and are slightly lower than the values displayed by comparable backarc rocks (Fig. 10C). Likewise, the La/Yb ratio of Cerro Silvia samples is well within arc rock values, whereas Cerro Bastión samples exhibit slightly higher values than our reference arc dataset (Fig. 10B). The Mitrauquén Formation samples show rare earth element concentrations, even higher than backarc rocks, and clear Eu negative anomalies (not present in Silvia and Bastión samples) and La/Yb ratios higher than both Silvia and Bastión samples (Fig. 10B–C).

As a summary, despite their position behind the current volcanic front (Fig. 2), Silvia and Bastión volcanic rocks have compositions more similar to the arc front than to the volcanic centers located behind the arc.

Please cite this article as: Tobal, J.E., et al., Middle to late Miocene extensional collapse of the North Patagonian Andes (41°30′–42°S), Tectonophysics (2015), http://dx.doi.org/10.1016/j.tecto.2015.06.032

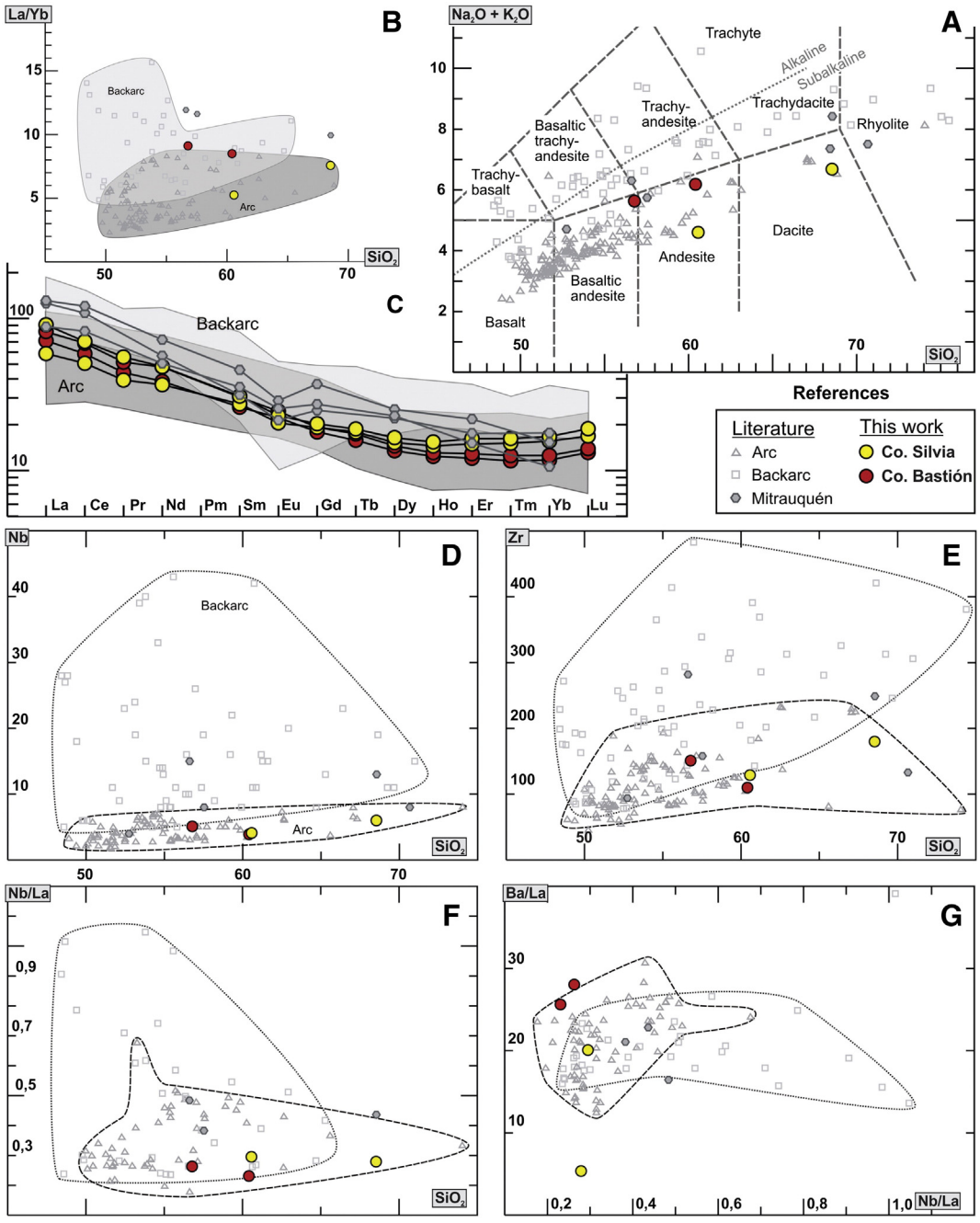

Fig. 10. Diagrams showing geochemical characteristics of the middle-late Miocene volcanic rocks studied in this work in comparison with compiled geochemical data in other late Pliocene to Quaternary arc and back-arc volcanic rocks, and with partially coeval volcanic rocks of the Mitrauquén Formation (38°–39°S). A) TAS (Total alkalis vs. silica) classification diagram (Le Bas et al., 1986); B) Plot of La/Yb vs. SiO_2; C) chondrite normalized REE diagram; D–G) plots of Nb (D), Zr (E), Nb/La (F) and Ba/La (G) vs. SiO_2 content (wt%).

4. Topographic analysis of the fold and thrust belt

4.1. Methods

Swath-averaged topographic profiles have proven to be a useful way to characterize the topography of orogenic belts in a variety of tectonic settings (Isacks, 1992; Masek et al., 1994; Bookhagen and Burbank, 2006; Berger and Spotila, 2008; Thomson et al., 2010; Ponza et al., 2010; among many others).

In order to quantify the topography of the Ñirihuau fold and thrust belt, we constructed five E–W topographic swath profiles spaced at 35 km (41°14′, 41°33′, 41°52′, 42°10′ and 42°30′) (Figs. 11A and 12A–E). These topographic transects, oriented perpendicularly to the main N-trending thrusts, extend for ~170 km, from the Liquiñe–Ofqui Fault Zone to the foreland area, encompassing the Cerro Bastión and Cerro Silvia volcanic depocenters. In addition, a roughly N–S topographic transect was constructed oriented parallel to the trace of the *Hielo Azul thrust* (Figs. 11A and 12F). We also constructed two local-scale E–W, 50 km-long, swath profiles that cross the Cerro Silvia and Cerro Bastión areas (Fig. 11D–E).

Swath profiles were extracted from the 90-m SRTM data. Following Sternai et al. (2011), we estimated an optimal 20-km-wide swath by using a semi-variogram analysis of the elevation data. Furthermore, this value largely insures the capture of the minimum and maximum elevations of all major drainage basins (Molin et al., 2004). We also calculated topographic volumes for each topographic swath profile, obtaining an indirect estimation of the orogenic volume created during the evolution of the Ñirihuau fold and thrust belt (Fig. 11B) (for further

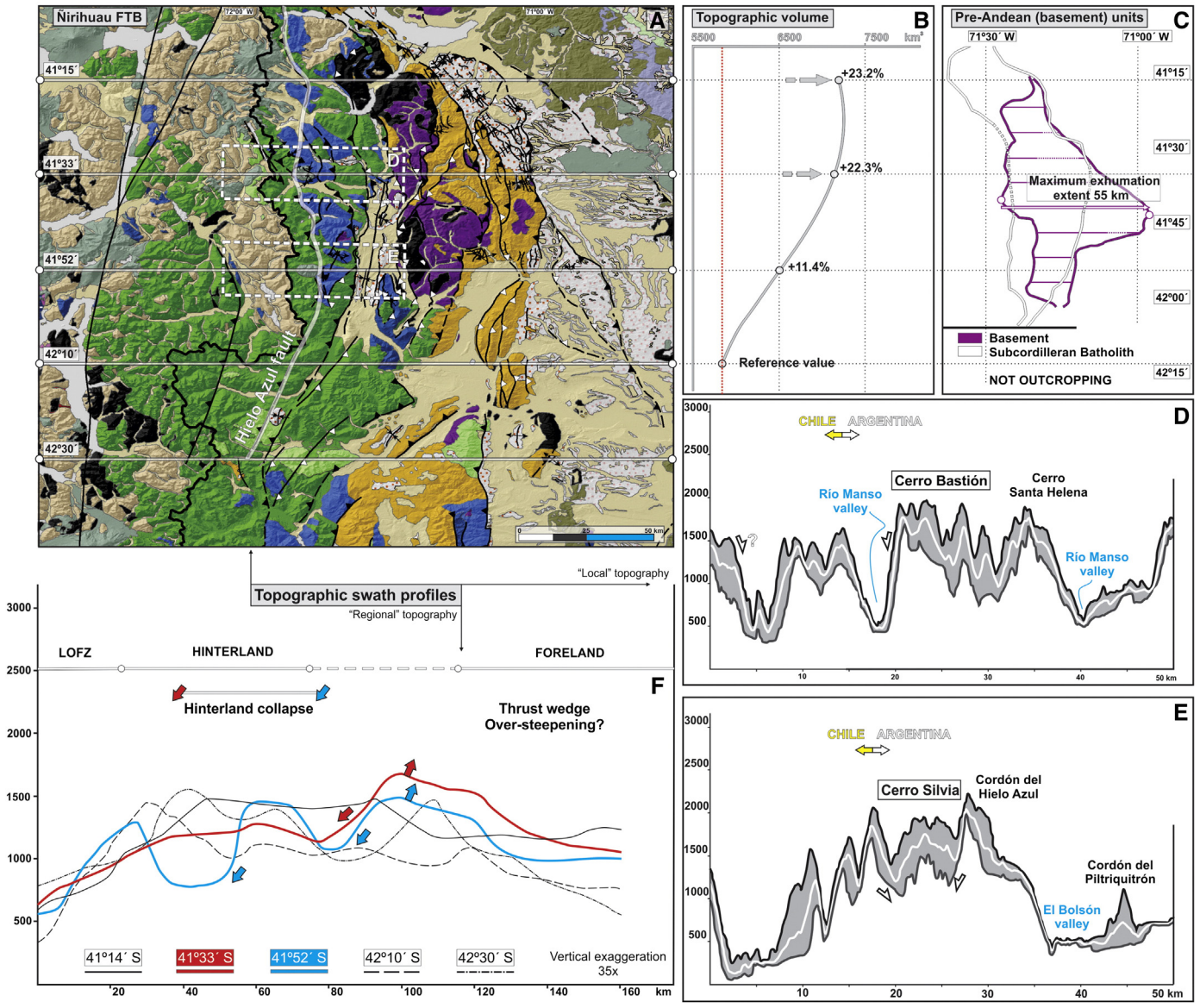

Fig. 11. Topographic analysis of the Ñirihuau fold and thrust belt. A) Location map showing the extent of both regional E–W 20 km width and local (Cerro Silvia and Cerro Bastión areas) topographic swath profiles (translucent white line); B) topographic volumes calculated for the selected swath profiles; C) surface distribution of pre-Andean units (basement and Subcordilleran Patagonian Batholith) across the fold and thrust belt showing a relationship between maximum topographic volumes and the maximum foreland extent of these units; D-E) local-scale topographic swath profiles at the Cerro Silvia and Cerro Bastión areas; F) mean elevation values along the regional-scale topographic swath profiles, showing that, in the 41°30′–42°S interval, there is a good correlation between a depressed zone at the hinterland and an over-steepened orogenic taper (see text for further details).

details about techniques used in this section, see Supplementary Material, Appendix C).

4.2. Results

The Ñirihuau fold and thrust belt presents an approximately symmetric parabolic shape (*sensu* Macedo and Marshak, 1999) with the apex (maximum foreland extent of the deformational front) at ~41°45′ (Figs. 2 and 11A). Since the pre-Miocene topography is unknown, the topographic volumes calculated here cannot be directly interpreted as the result of the last mountain building stage, and therefore interpretations based on these data require caution. However, a clear increment of the topographic volume in the northern part of the Ñirihuau fold and thrust belt emerges from these data (Fig. 11B). This pattern partially matches shortening values recently obtained by Orts et al. (2015) and also correlates closely with exposures of Paleozoic to Early Jurassic units through the sub-Andean region (Fig. 12C), which could be suggesting a relation between topography, shortening and exhumation.

The analysis of local-scale topographic swath profiles shows a direct correlation between the location of the studied volcanic sequences and negative topographic anomalies. At Cerro Silvia area, both the eastern normal fault that controlled the emplacement of middle Miocene volcanic units (i.e., the *Hielo Azul thrust*; see Fig. 5) and the inferred western fault are revealed by the swath profiles (Fig. 11E). To the north, in Cerro Bastión area, volcanic units are slightly shifted to the east with respect to an abrupt topographic break. However, during fieldwork this volcanic sequence was also recognized to the west (although it has not been studied in detail yet), coinciding with another topographic break visible in the swath (indicated with a question mark; see Fig. 11D), which might be reflecting a wider negative topographic anomaly in this area.

A first observation when comparing regional-scale swath profiles (mean elevation values tendency) is the existence of an anomalous, depressed-to-the-hinterland zone between 41°30′ and 41°45′, where syn-extensional volcanic activity has been recognized (Fig. 11F). These

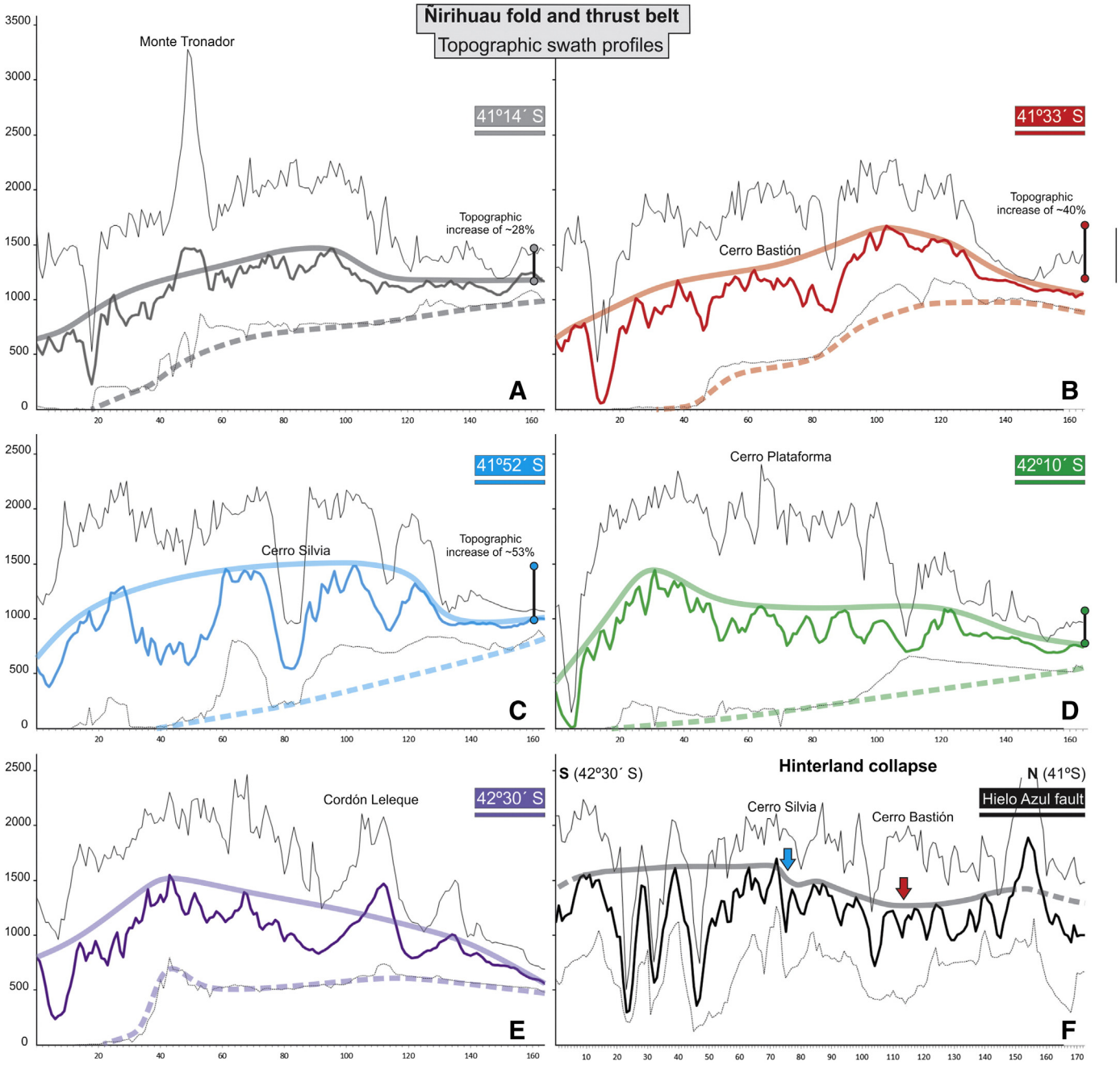

Fig. 12. Topographic swath profiles of the Ñirihuau fold and thrust belt (see location on Fig. 11A). A–E) E–W swath profiles from ~41°14′ to ~42°30′ S; F) swath profile computed along the inferred trace of the *Hielo Azul fault*. Maximum (thin solid black line), mean (thick solid colored line) and minimum (thin dotted black line) elevation profile curves are represented for each swath profile. Thick translucent solid and dashed lines reflect mean and minimum elevation data tendencies respectively.

anomalous topographic patterns involve significantly higher elevations at the eastern domain of the Ñirihuau fold and thrust belt (Fig. 11F). In addition, there are subtle differences between 41°30′ and 41°45′ S elevation patterns. A topographic depressed hinterland zone is much more evident for the 41°30′S swath profile (i.e., in the Cerro Bastión area).

A careful analysis of individual swath profiles reveals some important features (Fig. 12A–E). First, a negative-to-the-hinterland pattern of elevations is only visible for 41°14′, 41°30′ and 41°45′ S swath profiles (42°10′ and 42°30′ S swath profiles show opposite patterns). Second, the foreland/eastern domain increase in elevations is much higher for the 41°30′ and 41°45′ S than for the 41°14′ S swath profile. Third, the transition from higher foreland/eastern domain elevations to lower western domain is abrupt for the 41°30′ and 41°45′ S swath profiles (i.e., it occurs in a narrow segment), while is smooth in the case of the 41°14′ S swath profile. Finally, the analysis of the roughly N–S topographic swath profile allow identifying a subtle depression of topography at Cerro Silvia and Cerro Bastión volcanic depocenters, which is again more pronounced in the case of Cerro Bastión.

5. Discussion

5.1. A new volcanic event along the main axis of the North Patagonian Andes

Cerro Silvia and Cerro Bastión volcanic rocks exposed at the western sector of the Ñirihuau fold and thrust belt were diachronously erupted during middle to late Miocene times, and not in the Oligocene as was

previously postulated (Diez and Zubia, 1981; Giacosa et al., 2001). This volcanic event would have started at ~41°45′ S at 15 Ma ceasing by ~7 Ma at 41°30′ S. A comparable K–Ar age was reported for the Cerro Plataforma volcanic rocks to the south (Lizuaín, 1983), but these show no evidence of associated normal faulting.

To the north, between 38° and 39°S, partially coeval (~9.5–8 Ma) volcanic rocks of the Mitrauquén Formation were emplaced along the main axis of the Andes (Suárez and Emparán, 1997), and were interpreted as a syn-compressional unit (Melnick et al., 2006). These rocks lie conformably above the late Oligocene to early Miocene Cura Mallín Formation (partly contemporaneous to the Ñirihuau Formation; Burns et al., 2006) and are unconformably capped by the early Pliocene to early Pleistocene Cola de Zorro Formation (Vergara and Muñoz, 1982; Suárez and Emparán, 1997; Lara et al., 2001). Even though stratigraphic relations are very similar, the late Miocene volcanic sections described in this work would be related to a different tectonic regime (i.e., the westernmost Andean zone between 41° and 42°S would have undergone particular conditions that are not described elsewhere).

5.2. Evidences of a late orogenic extensional event and possible implications on the topography

We described in the previous sections field evidence that points to an extensional control of the studied volcanic depocenters. The structural analysis revealed the existence of progressive unconformities in association with normal faults in Cerro Silvia (Fig. 5) and Cerro Bastión (Fig. 8). In order to complement these observations, we have performed a topographic analysis that evidenced a correlation between topography and extensional structures. Topographic swath profiles through the Cerro Silvia and Cerro Bastión areas exhibit negative topographic anomalies where normal faults that limit both volcanic depocenters are located. Regional-scale swath profiles at 41°14′ and 41°45′ S present a depressed-to-the-hinterland (western domain of fold and thrust belt) topographic profile that involves anomalously high altitudes at the transition between the eastern domain of fold and thrust belt and the foreland zone. Two facts arise from the analysis of these swath profiles. First, this hinterland-depressed zone can be identified in both the E–W profiles and the N–S profile and closely matches the area interpreted here as affected by late Miocene extensional tectonics. Second, the topographic pattern of the 41°14′ and 41°45′ S swath profiles differs significantly from the neighbor segments (Fig. 12).

Then, as a first approach, we propose that these along-strike differences in topography could be the result of a complex spatio-temporal pattern of structural evolution of the Ñirihuau fold and thrust belt, as recently described in other parts of the Andes (see for example Strecker et al., 2007, 2009; Giambiagi et al., 2009; Hain et al., 2011; Parra et al., 2012; Pearson et al., 2013). These disparate spatio-temporal patterns of deformation strongly control sediment dynamics and consequently erosional processes, which in turn can influence the evolution of the thrust wedge (Berger and Spotila, 2008; Whipple, 2009, and references therein). In the next section, we discuss some constraints about magmatism and deformation during middle to late Miocene times through the fold and thrust belt, to assess whether this topographic pattern could develop in response to tectonic forcing or not. Since erosional (particularly glacial) processes have not been fully studied in the area, we can only speculate about the relative importance of climatic forcing on the development of the accretionary wedge. Further studies will be necessary to assess this key point.

5.3. Magmatism and deformation in the hinterland zone of the fold and thrust belt

Synorogenic sequences accumulated from the eastern domain of the fold and thrust belt to the foreland zone indicate an early to middle Miocene compressive stage beginning at the main Andes, although there is still no straightforward thrust belt propagation model (Orts et al., 2012; Bilmes et al., 2013; Bechis et al., 2014; Ramos et al., 2014; Fig. 13A–B). Geochronological and termochronological data from the Chilean slope of the Andes indicate contemporaneous and incipient late early Miocene magmatic activity at the LOFZ from 41°S to the south (Adriasola et al., 2006; Thomson, 2002). Extensive outcrops of younger, middle to late Miocene plutonic bodies mainly exposed from 41°45′S to the north, indicate that this magmatic activity then intensified and expanded to the east. The magmatic activity expansion between 41° and 41°25′ S is represented by 15 to 8 Ma plutonic bodies outcropping at the eastern slope of the Andes (González Díaz and Valvano, 1978; Rapela et al., 1987; Aragón et al., 2012; Fig. 13A).

On the other hand, new geochronological and geochemical data presented in this study indicate that arc-related volcanism started along the Andean axis, in Cerro Silvia area at ~15 Ma and then migrated northward to Cerro Bastión area at ~7 Ma. This fact indicates a spatial and temporal relation between this volcanic event and the last phase of pluton emplacement of the North Patagonian Batholith (Pankhurst et al., 1999). The analyzed volcanic sequences constitute, together with Cerro Plataforma volcanic rocks (15 Ma; Lizuaín, 1983), the only volcanic products recognized at the hinterland zone until late Miocene-early Pliocene times (Lara et al., 2001). The structural and geochemical data presented in this paper clearly indicate the synextensional character of these middle to late Miocene volcanic sequences, constituting an example of synconvergent hinterland extension. As stated above, this would not be the case of Cerro Plataforma volcanic rocks. During Plio-Quaternary times, tectonomagmatic processes concentrated in the LOFZ to the west (Cembrano et al., 1996, 2000; Thomson, 2002; Adriasola et al., 2006).

Moreover, the topographic analysis also revealed that the Ñirihuau fold and thrust belt experienced maximum deformation at the latitudes where magmatism migrated to the east. Several studies had already documented the relation between magmatic activity and compressional deformation for other mountain systems in the world (Kalakay et al., 2001; Galland et al., 2003; Tibaldi, 2008; Tibaldi et al., 2009; Gonzalez et al., 2009; see Tibaldi et al., 2010, and Ferré et al., 2012, for a review). Particularly, Gonzalez et al. (2009) showed field evidence supporting the hypothesis of magma emplacement along synchronous reverse faults, as proposed by Tibaldi (2008) and modeled by Ferré et al. (2012). Similarly, Kalakay et al. (2001) had revealed the mechanisms of emplacement of intrusive bodies in frontal thrust ramps in the Sevier fold and thrust belt. We therefore speculate that expansion of the middle to late Miocene magmatic activity would have been associated with the stacking of crustal thrust sheets north of 41°30′S that led to higher shortenings (and consequently higher topographic volumes) in this region. These thrust faults could have provided preferential pathways for magma ascent, that not only controlled the emplacement of plutons, but also the extrusion of magma during the inversion of the structures at Cerro Bastión and Cerro Silvia depocenters.

Two important questions, however, remain unanswered. Why was shortening more intense at the northern end of the fold and thrust belt, and why was this volcanic activity only manifested between 41°45′ and 41°30′ S? To answer this, we consider that it is crucial to assess the correlation between along-strike differences in topography and location of the middle to late Miocene synextensional volcanism. We have also shown associated along-strike variations in the middle to late Miocene deformational and magmatic pattern. Following the approach of DeCelles and Mitra (1995) (i.e., a not strictly quantifiable appraisal of the state of the wedge—subcritical, critical or supercritical—through time), we hypothesize that depressed-to-the-hinterland topographic profiles described above could be reflecting along-strike variations in the wedge taper behavior. We envisage anomalously high altitudes at the transition between the eastern domain of the fold and thrust belt and the foreland zone as a possible evidence of an over-steepening of the taper (supercritical state of the thrust wedge). This is one of the mechanisms proposed for explaining synconvergent extensional events (see Wells et al., 2012, and references therein).

Please cite this article as: Tobal, J.E., et al., Middle to late Miocene extensional collapse of the North Patagonian Andes (41°30′–42°S), Tectonophysics (2015), http://dx.doi.org/10.1016/j.tecto.2015.06.032

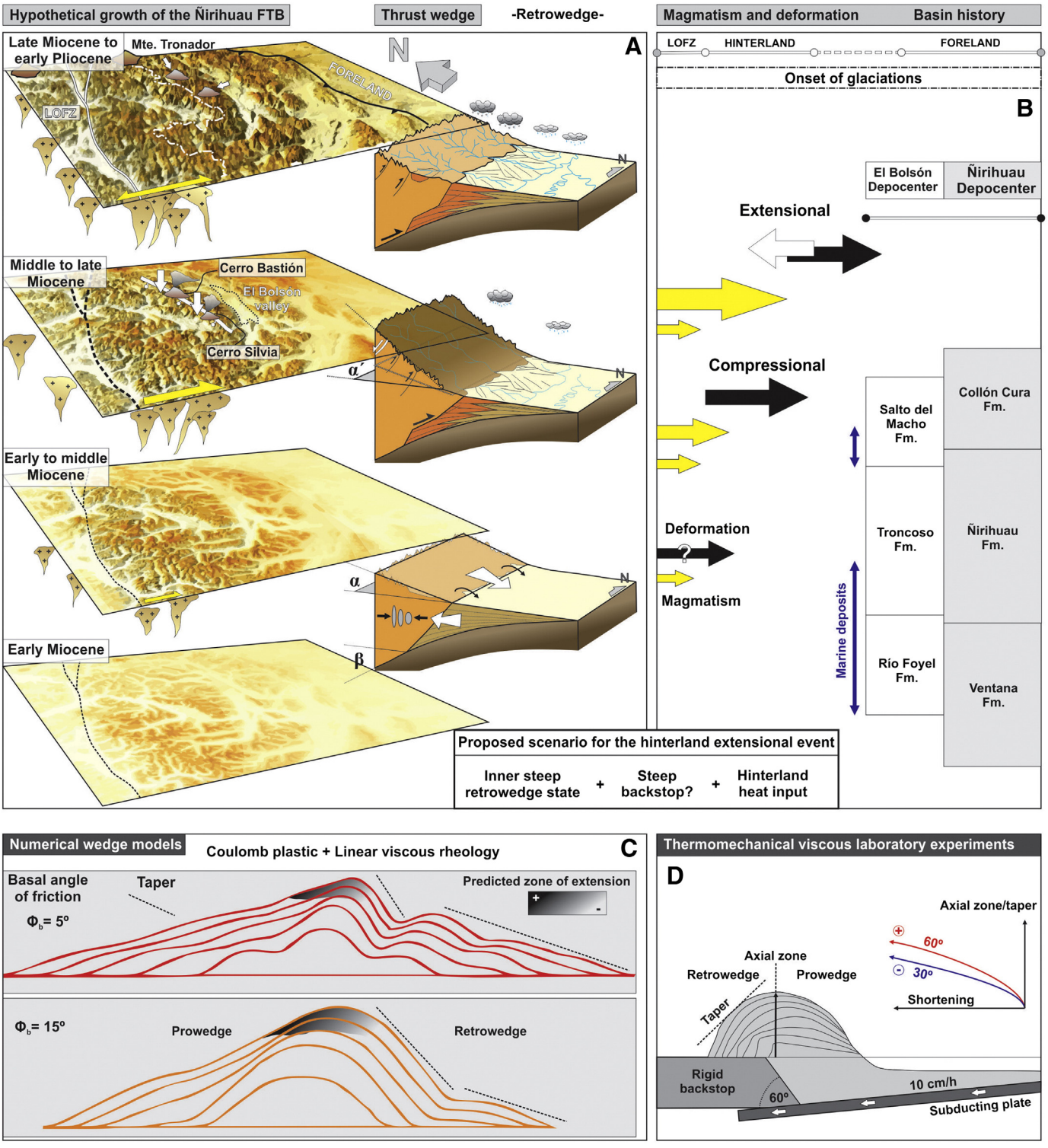

Fig. 13. Summary diagram discussing the Miocene evolution of the North Patagonian Andes. A) Hypothetical spatial and temporal evolution of the Ñirihuau fold and thrust belt and wedge thrust development through time. B) Schematic diagram representing main deep and surface processes recording fold and thrust development: magmatism, deformation and basin evolution (mainly based on Bechis et al., 2014, and our own data). C) Numerical models of Willet (1999) that investigate rheological dependence of extension in thrust wedge systems. Both panels (gray background) are redrawn from examples of a Coulomb plastic behavior of the wedge; gray scale bar schematically represents the zones where extension develops when a linear viscous rheology is considered. D) Thermomechanical experiments evaluating the influence of a backstop dip and convergence velocity during wedge development (Rossetti et al., 2002). A case example with a maximum backstop dip (60°) and convergence velocity (10 cm/h) that leads to a steep retrowedge taper angle that contribute to an over-steepening of the taper wedge (supercritical state of a wedge proposed in this paper as an extensional triggering factor; see text for further details).

As stated before, we cannot estimate neither the importance of erosional forcing on the development of this orogenic wedge nor the possibility of climate-controlled gradients in altitudes through the fold and thrust belt. The role of glaciation on topographic evolution of mountain belts, e.g. whether the net effect of glacial erosion increase or decrease orogenic relief, is now subject of intense debate (Egholm et al., 2009; Sternai et al., 2012; Thomson et al., 2010; Valla et al., 2011). We think that structural data presented in this paper are robust enough to

Please cite this article as: Tobal, J.E., et al., Middle to late Miocene extensional collapse of the North Patagonian Andes (41°30′–42°S), Tectonophysics (2015), http://dx.doi.org/10.1016/j.tecto.2015.06.032

propose a tectonic control on topography. Further studies will be necessary to better understand the role of glacial erosion during Plio-Quaternary evolution of topography in the area.

To evaluate the hypothesis of a possible supercritical state of the wedge taper as an effective mechanism triggering extension at this Andean segment, we turn to analogue and numerical models and thermomechanical experiments performed for doubly-vergent orogenic wedges (Buck and Sokoutis, 1994; Wang and Davis, 1996; Willet, 1999; Rossetti et al., 2002; Fig. 13C–D). Three main constraints can be pointed out. First, Coulomb wedge (plastic behavior) numerical models lead to the development of two distinct retrowedge taper profiles (an inner steeper one and an outer *critical* taper; see Wang and Davis, 1996; Willet, 1999, and references therein). No horizontal extension at upper crustal levels is observed under these conditions (Fig. 13C). Second, a steeper retrowedge profile is favored either by the effect of a high-angle rigid backstop at the foreland zone or by a high convergence velocity (Rossetti et al., 2002; Fig. 13D). Third, surface extension occurs in the wedge thrust system next to its axial region only when viscous mechanisms dominate the wedge behavior, which is in turn expected when higher temperatures are achieved (Buck and Sokoutis, 1994; Willet, 1999).

The Ñirihuau fold and thrust belt could be a case where these conditions were reproduced. The described higher Miocene shortening north of 41°45′ S could have led the retrowedge into a supercritical state, as suggested by the topographic analysis. This higher stacking of crustal thrust sheets north of 41°30′S producing strong load subsidence was recently proposed to explain the marine influence recorded in the synorogenic sequences deposited at the northern end of the El Bolsón sub-basin (Bechis et al., 2014). The existence of an effective backstop in the northern end of the Ñirihuau fold and thrust belt (i.e., the North Patagonian Massif; see Figs. 1, 2, 3 and 11A) could have also contributed to this scenario. Since magmatism coexisted with deformation during middle to late Miocene times, an increase in geothermal gradient could constitute the critical factor in the development of extension in these models, promoting a viscous behavior of the thrust wedge.

Since geological materials in the crust inevitably show a more complex behavior than predicted by models (Willet, 1999), caution is required when assessing the mechanisms that could have triggered synextensional volcanism in this area (for further considerations about the extent of applicability of these models to natural examples, the reader is referred to those papers).

A common, recently modeled mechanism explaining synconvergent extension is slab rollback (Sternai et al., 2014; Wells et al., 2012). Since Orts et al. (2015) recently interpreted the migration of magmatic activity north of 41°45′S as a possible case of a shallowing-retreating cycle of the subducted slab, this could constitute an alternative explanation for the extensional event described in this work. However, this seems to constitute a case of localized upper-crustal synconvergent extension (Long et al., 2015) rather than a crustal-scale orogenic process as expected from rollback hypothesis.

6. Conclusions

Cerro Silvia and Cerro Bastión volcanic rocks hosted in the inner sector of the North Patagonian Andes are synextensional arc-related products erupted during middle to late Miocene times, as revealed by the new geochronological data and the structural analysis. This extensional event occurred during and after compressional tectonics in the area.

The topographic analysis performed in this work also provides valuable insights about this event. Regional-scale swath profiles show a hinterland depressed zone between 41°45′ and 41°30′ S, so coincident with the areas of synextensional volcanism. Anomalously high altitudes at the transition zone between the eastern domain of the fold and thrust belt and the foreland can be potentially related to along-strike variations in the wedge taper angle.

We propose that over-steepening of the taper (thrust wedge supercritical state) could be an effective mechanism triggering extension in the inner sector of this Andean segment. To support this hypothesis, we have evaluated analogue and numerical models and thermomechanical experiments that address the conditions under which surface extension in a thrust wedge can occur. This volcanic event shows a clear spatial and temporal relation with the last phase of pluton emplacement of the North Patagonian Batholith. We hypothesize that this magmatism, associated with high heat flows, could have promoted a viscous behavior of the thrust wedge that could have led to extension in the inner sector of the evolving fold and thrust belt.

Acknowledgments

We acknowledge Pietro Sternai and Alessandro Tibaldi for their reviews, which significantly improved this study. Thanks to the Editor Laurent Jolivet. We acknowledge Guido Gianni for creative discussions that significantly improved preliminary versions of this paper. We are also grateful to Emiliano Renda, Bruno Colavitto, Andrés Echaurren and Pedro Kleiman for all the help and support during fieldwork. This work was financed by PIP 11220110100506, UBACYT 20020110100019, PICT-2012-1490 Proyects. This is the R-163 contribution of the Instituto de Estudios Andinos “Don Pablo Groeber”.

Appendix A. Supplementary data

Supplementary data associated with this article can be found in the online version at http://dx.doi.org/10.1016/j.tecto.2015.06.032. These data include the Google map of the most important areas described in this article.

References

Adriasola, A.C., Thomson, S.N., Brix, M.R., Hervé, F., Stöckhert, B., 2006. Postmagmatic cooling and late Cenozoic denudation of the North Patagonian Batholith in the Los Lagos region of Chile, 41°–42°15′S. Int. J. Earth Sci. 95 (3), 504–528.

Aragón, E., Castro, A., Díaz-Alvarado, J., Liu, D.-Y., 2012. The North Patagonian Batholith at Paso Puyehue (Argentina–Chile). SHRIMP ages and compositional features. J. S. Am. Earth Sci. 32 (4), 547–554.

Bechis, F., Cristallini, E.O., 2006. Inflexiones en estructuras del sector norte de la faja plegada y corrida de Ñirihuau, provincia de Río Negro. Rev. Asoc. Geol. Argent. 25, 18–25.

Bechis, F., Encinas, A., Concheyro, A., Litvak, V.D., Aguirre-Urreta, B., Ramos, V.A., 2014. New Age constraints for the Cenozoic marine transgressions of northwest Patagonia, Argentina (41°–43° S): paleogeographic and tectonic implications. J. S. Am. Earth Sci. 52, 72–93.

Berger, A.L., Spotila, J.A., 2008. Denudation and deformation in a glaciated orogenic wedge: the St. Elias orogeny, Alaska. Geology 36, 523–526.

Bilmes, A., D'Elía, L., Franzese, J.R., Veiga, G.D., Hernández, M., 2013. Miocene block uplift and basin formation in the Patagonian foreland: the Gastre Basin, Argentina. Tectonophysics 601, 98–111.

Bookhagen, B., Burbank, D.W., 2006. Topography, relief, and TRMM-derived rainfall variations along the Himalaya. Geophys. Res. Lett. 33. http://dx.doi.org/10.1029/2006GL026037.

Buck, W.R., Sokoutis, D., 1994. Analogue model of gravitational collapse and surface extension during continental convergence. Nature 369, 737–740.

Burns, W.M., Jordan, T.E., Copeland, P., Kelley, S.A., 2006. The case for extensional tectonics in the Oligocenee Miocene Southern Andes as recorded in the Cura Mallín basin (36°–38° S). In: Kay, S.M., Ramos, V.A. (Eds.), Evolution of an Andean Margin: A Tectonic and Magmatic View from the Andes to the Neuquén Basin (35°–39° lat). Geological Society of America Special Paper 407, pp. 163–184.

Castro, A., Moreno-Ventas, I., Fernández, C., Vujovich, G., Gallastegui, G., Heredia, N., Martino, R.D., Becchio, R., Corretgé, L.G., Díaz-Alvarado, J., Such, P., García-Arias, M., Liu, D.-Y., 2011. Petrology and SHRIMP U–Pb zircon geochronology of Cordilleran granitoids of the Bariloche area, Argentina. J. S. Am. Earth Sci. 32 (4), 508–530.

Cazau, L., Mancini, D., Cangini, J., Spalletti, L., 1989. Cuenca de Ñirihuau. In: Chebli, G., Spalletti, L. (Eds.), Cuencas Sedimentarias ArgentinasSerie Correlación Geológica 6. Tucumán, pp. 299–318.

Cembrano, J., Hervé, F., Lavenu, A., 1996. The Liquifie Ofqui fault zone: a long-lived intra-arc fault system in southern Chile. Tectonophysics 259, 55–66.

Cembrano, J., Schermer, E., Lavenu, A., Sanhueza, A., 2000. Contrasting nature of deformation along an intra-arc shear zone, the Liquiñe-Ofqui fault zone, southern Chilean Andes. Tectonophysics 319, 129–149.

Dalla Salda, L., Cingolani, C., Varela, R., 1991. El basamento cristalino de la región nordpatagónica de los lagos Gutiérrez, Marcardi y Guillelmo, Provincia de Río Negro. Rev. Asoc. Geol. Argent. 46 (3-4), 263–276.

Please cite this article as: Tobal, J.E., et al., Middle to late Miocene extensional collapse of the North Patagonian Andes (41°30′–42°S), Tectonophysics (2015), http://dx.doi.org/10.1016/j.tecto.2015.06.032

DeCelles, P.G., Mitra, G., 1995. History of the Sevier orogenic wedge in terms of critical taper models, northeast Utah and southwest Wyoming. Geol. Soc. Am. Bull. 107, 454–462.
De La Cruz, R., Suárez, M., Belmar, M., Quiroz, D., Bell, M., 2003. Geología del área Coihaique-Balmaceda, Región de Aisén del General Carlos Ibáñez del Campo (1: 100.000). Servicio Nacional de Geologíay Minería. 80. SERNAGEOMIN, Serie Geología Básica, Santiago.
Diez, O., Zubia, M., 1981. Sinópsis estratigráfica de la región de El Bolsón, provincia de Río Negro. Rev. Asoc. Geol. Argent. 36 (1), 19–28.
Duhart, P., Crignola, G., Ordoñez, B.A., Muñoz, J., 2000. Franjas metalogénicas en Chiloé continental (41° –44° S). IX Congreso Geológico Chileno, Actas, pp. 201–205 (Puerto Varas).
Egholm, D.L., Nielsen, S.B., Pedersen, V.K., Lesemann, J.-E., 2009. Glacial effects limiting mountain height. Nature 460, 884–888.
Feruglio, E., 1947. Descripción Geológica de la Hoja 40b, San Carlos de Bariloche, Río Negro (1:200.000). Dirección Nacional de Geología y Minería, Buenos Aires.
Ferré, E.C., Galland, O., Montanari, D., Kalakay, T.J., 2012. Granite magma migration and emplacement along thrusts. Int. J. Earth Sci. 101 (7), 1673–1688.
Galland, O., de Bremond d'Ars, J., Cobbold, P.R., Hallot, E., 2003. Physical models of magmatic intrusion during thrusting. Terra Nova 15, 405–409.
García-Sansegundo, J., Farias, P., Gallastegui, G., Giacosa, R.E., Heredia, N., 2009. Structure of the Gondwanan basement in the Bariloche region (North Patagonian Argentine Andes). Int. J. Earth Sci. 98, 1599–1608.
Giacosa, R., Heredia, N., 2004. Structure of the North Patagonian thick-skinned fold-and-thrust belt, southern central Andes, Argentina (41°–42°S). J. S. Am. Earth Sci. 18 (1), 61–72.
Giacosa, R., Heredia, N., Césari, O., Zubia, M., González, R., Faroux, A., 2001. Descripción geológica de la Hoja 4172-IV, San Carlos de Bariloche, Provincias de Río Negro y Neuquén (1:250.000). Servicio Geológico Minero Argentino, Instituto de Geología y Recursos Minerales, Boletín. 279 p. 77 (Buenos Aires Argentina).
Giacosa, R.E., Afonso, J.C., Heredia, C., Paredes, J., 2005. Tertiary tectonics of the sub-Andean region of the North Patagonian Andes, southern central Andes of Argentina (41–42°30′S). J. S. Am. Earth Sci. 20 (3), 157–170.
Giambiagi, L., Ghiglione, M., Cristallini, E.O., Bottesi, G., 2009. Kinematic models of basement/cover interaction: Insights from the Malargüe fold and thrust belt, Mendoza, Argentina. J. Struct. Geol. 31 (12), 1443–1457.
Giovanni, M.K., Horton, B.K., Garzione, C.N., McNulty, B., Grove, M., 2010. Extensional basin evolution in the Cordillera Blanca, Peru: stratigraphic and isotopic records of detachment faulting and orogenic collapse in the Andean hinterland. Tectonics 29, 1–21.
Gonzalez, G., Cembrano, J., Aron, F., Veloso, E.E., Shyu, J.B.H., 2009. Coeval compressional deformation and volcanism in the central Andes, case studies from northern Chile (23° S–24° S). Tectonics 28 (6) (TC6003).
González Bonorino, F., 1944. Descripción geológica y petrográfica de la Hoja 41b, Río Foyel (Provincia de Río Negro). Dirección de Minería, Geología e Hidrogeología, Boletín. 56 p. 124.
González Bonorino, F., 1973. Geología del área entre San Carlos de Bariloche y Llao-Llao. 16. Fundación Bariloche, Publicación, San Carlos de Bariloche, pp. 1–53.
González Bonorino, F., 1974. La Formación Millaqueo y la «Serie Porfirítica» de la Cordillera Patagónica. Rev. Asoc. Geol. Argent. 29 (2), 145–154.
González Bonorino, F., González Bonorino, G., 1978. Geología de la región de San Carlos de Bariloche. Rev. Asoc. Geol. Argent. 33 (3), 175–210.
González Díaz, E., 1979. Estratigrafía del área de la Cordillera Patagónica entre los paralelos 40° 30′ y 41° 00′ de lati0074ud sur (provincia del Neuquén). VII Congreso Geológico Argentino I, pp. 525–537 (Buenos Aires.).
González Díaz, E.F., 1982. Chronological zonation of granitic plutonism in the northern Patagonian Andes of Argentina: the migration of intrusive cycles. Earth-Sci. Rev. 18, 365–393.
González Díaz, E.F., Lizuaín, A., 1984. El Complejo volcano-clástico y plutónico del sector cordillerano. In: Ramos, V. (Ed.), Geología y Recursos Naturales de la Provincia de Río Negro. 1 (5), pp. 119–129 (Buenos Aires).
González Díaz, E.F., Valvano, J., 1978. Plutonitas graníticas cretácicas y neoterciarias entre el sector norte del lago Nahuel Huapi y el lago Traful (provincia del Neuquén). VII Congreso Geológico Argentino. I pp. 227–242 (Neuquén).
Gordon, A., Ort, M., 1993. Edad y correlación del plutonismo subcordillerano en las provincias de Río Negro y Chubut. XII Congreso Geológico Argentino. IV pp. 120–127 (Mendoza).
Hain, M.P., Strecker, M.R., Bookhagen, B., Alonso, R.N., Pingel, H., Schmitt, A.K., 2011. Neogene to Quaternary broken foreland formation and sedimentation dynamics in the Andes of NW Argentina (25 S). Tectonics 30 (TC2006).
Halpern, M., Stipanicic, P., Toubes, R., 1975. Geocronología (Rb/Sr) en los Andes Australes Argentinos. Rev. Asoc. Geol. Argent. 30 (2), 180–192.
Hervé, M., 1976. Estudio Geológico de la Falla Liquiñe-Reloncaví en el área de Liquiñe: antecedentes de un movimiento transcurrente. I Congreso Geológico Chileno. I pp. B39–B56 (Santiago).
Hervé, F., Pankhurst, R.J., Fanning, C.M., Calderon, M., Yaxley, G.M., 2007. The South Patagonian batholith: 150 my of granite magmatism on a plate margin. Lithos 97, 373–394.
Isacks, B.L., 1992. Long term land surface processes: erosion, tectonics and climate history in mountain belts. In: Mather, P.M. (Ed.), TERRA-1: Understanding the Terrestrial Environment. Taylor and Francis, London, pp. 21–36.
Jarrard, R.D., 1986. Relations among subduction parameters. Rev. Geophys. 24, 217–284.
Kalakay, T.J., John, B.E., Lageson, D.R., 2001. Fault-controlled pluton emplacement in the Sevier fold-and-thrust belt of southern Montana. J. Struct. Geol. 23, 1151–1165.
Lange, D., Cembrano, J., Rietbrock, A., Haberland, C., Dahm, T., Bataille, K., 2008. First seismic record for intra-arc strike–slip tectonics along the Liquiñe–Ofqui fault zone at the obliquely convergent plate margin of the southern Andes. Tectonophysics 455 (1-4), 14–24.
Lara, L.E., Rodríguez, C., Moreno, H., Pérez de Arce, C., 2001. Geocronología K–Ar y geoquímica del volcanismo plioceno superior-pleistoceno de los Andes del Sur (39°–42°S). Rev. Geol. Chile 28, 67–90.
Lavenu, A., Cembrano, J., 1999. Compressional-and transpressional-stress pattern for Pliocene and Quaternary brittle deformation in fore arc and intra-arc zones (Andes of central and southern Chile). J. Struct. Geol. 21 (12), 1669–1691.
Le Bas, M.J., Le Maitre, R.W., Streckeisen, A., Zanettin, B., 1986. A chemical classification of volcanic rocks based on the total alkali–silica diagram. J. Petrol. 27, 745–750.
Lizuaín, A., 1980. Las formaciones Suprapaleozoicas y Jurásicas de la Cordillera Patagónica. Provincias de Río Negro y Chubut. Rev. Asoc. Geol. Argent. 35 (2), 174–186.
Lizuaín, A., 1981. Características y edad del plutonismo en los alrededores del lago Puelo. Provincia del Chubut. VIII Congreso Geológico Argentino. III pp. 607–616 (Buenos Aires Argentina).
Lizuaín, A., 1983. Descripción geológica de la Hoja 42a y b El Maitén, Provincia de Río Negro. Servicio Geológico Nacional, unpublished report, Buenos Aires (Argentina).
Lizuaín, A., Viera, R., 2010. Descripción geológica de la Hoja 4372-I y II, Esquel, Provincia de Chubut. Servicio Geológico Minero Argentino, Instituto de Geología y Recursos Minerales, Boletín. 369 pp. 1–92 (Buenos Aires, Argentina).
Long, S.P., Thomson, S.N., Reiners, P.W., Di Fiori, R.V., 2015. Synorogenic extension localized by upper-crustal thickening: an example from the Late Cretaceous Nevadaplano. Geology 43 (4), 351–354.
Lonsdale, P., 2005. Creation of the Cocos and Nazca plates by fission of the Farallon plate. Tectonophysics 404, 237–264.
López-Escobar, L., Parada, M.A., Moreno, H., Frey, F., Hickey-Vargas, R., 1992. A contribution to the petrogenesis of Osorno and Calbuco volcanoes, Southern Andes (41°00′–41°30′S): comparative study. Rev. Geol. Chile 19 (2), 211–226.
López-Escobar, L., Kilian, R., Kempton, P.D., Tagiri, M., 1993. Petrography and geochemistry of Quaternary rocks from the Southern Volcanic Zone of the Andes between 41°30′ and 46°00′S, Chile. Rev. Geol. Chile 20 (1), 35–55.
López-Escobar, L., Parada, M.A., Hickey-Vargas, R., Frey, F.A., Kempton, P.D., Moreno, H., 1995. Calbuco Volcano and minor eruptive centers distributed along the Liquiñe–Ofqui Fault Zone, Chile (41°–-42° S): contrasting origin of andesitic and basaltic magma in the Southern Volcanic Zone of the Andes. Contrib. Mineral. Petrol. 119 (4), 345–361.
Macedo, J.M., Marshak, S., 1999. Controls on the geometry of fold-thrust belt salient. Geol. Soc. Am. Bull. 111, 1808–1822.
Maloney, K.T., Clarke, G.L., Klepeis, K.A., Quevedo, L., 2013. The Late Jurassic to present evolution of the Andean margin: drivers and the geological record. Tectonics 32 (5), 1049–1065.
Mancini, D., Serna, M., 1989. Evaluación petrolera de la Cuenca de Ñirihuau. I Congreso Nacional de Exploración de Hidrocarburospp. 739–762.
Masek, J.G., Isacks, B.L., Gubbels, T.L., Fielding, E.J., 1994. Erosion and tectonics at the margins of continental plateaus. J. Geophys. Res. 99 (B7), 941–956.
Massaferro, G.I., Haller, M.J., D'Orazio, M., Alric, V.I., 2006. Sub-recent volcanism in Northern Patagonia: a tectonomagmatic approach. J. Volcanol. Geotherm. Res. 155 (3-4), 227–243.
Mazzoni, M., Benvenuto, A., 1990. Radiometric ages of Tertiary ignimbrites and the Collón Curá Formation northwestern Patagonia. XI Congreso Geológico Argentino, 87–90, San Juan.
McNulty, B.A., Farber, D.L., 2002. Active detach-ment faulting above the Peruvian flat slab. Geology 30 (6), 567–570.
Mella, M., Muñoz, J., Vergara, M., Klohn, E., Farmer, L., Stern, C., 2005. Petrogenesis of the Pleistocene Tronador volcanic group, Andean Southern Volcanic Zone. Rev. Geol. Chile 32 (1), 131–154.
Melnick, D., Rosenau, M., Folguera, A., Echtler, H., 2006. Neogene Tectonics of the Western flank of the Neuquén Andes, 37°–39°30′ S. In: Kay, S.M., Ramos, V.A. (Eds.), Evolution of an Andean Margin: A Tectonic and Magmatic View from the Andes to the Neuquén Basin (35–39° S). Special Paper Geological Society of America 407, pp. 73–95.
Molin, P., Pazzaglia, F.J., Dramis, F., 2004. Geomorphic expression of active tectonics in a rapidly-deforming forearc, Sila Massif, Calabria, southern Italy. Am. J. Sci. 304, 559–589.
Muñoz, J., 1988. Volcanismo Mioceno superior (Tortoniano) en la región del Alto BíoBío. V Congreso Geológico Chileno. III pp. 275–296 (Santiago).
Muñoz, J., Stern, C., 1988. The Quaternary volcanic belt of the Southern continental margin of South America: transverse structural and petrochemical variations across the segment between 38° S and 39° S. J. S. Am. Earth Sci. 1, 147–162.
Muñoz, J., Stern, C., 1989. Alkaline magmatism within the segment 38°–39°S of the Plio-Quaternary volcanic belt of the Southern South American continental margin. J. Geophys. Res. 94 (B4), 4545–4560.
Orts, D., Folguera, A., Encinas, A., Ramos, M., Tobal, J., Ramos, V., 2012. Tectonic development of the North Patagonian Andes and their related Miocene foreland basin (41°30′–43° S). Tectonics 31 (TC3012).
Orts, D., Folguera, A., Giménez, M., Ruiz, F., Rojas Vera, E., Lince Klinger, F., 2015. Cenozoic building and deformational processes in the North Patagonian Andes. J. Geodyn. 86, 26–41.
Pankhurst, R.J., Weaver, S.D., Hervé, F., Larrondo, P., 1999. Mesozoic–Cenozoic evolution of the North Patagonian Batholith in Aysen, southern Chile. J. Geol. Soc. 156 (4), 673–694.
Pankhurst, R.J., Hervé, F., Fanning, M., Suárez, M., 2003. Coeval plutonic and volcanic activity in the Patagonian Andes: the Patagonian Batholith and the Ibáñez and Divisadero Formations, Aisén, southern Chile. X Congreso Geológico Chileno, Actas, CD-ROM, Concepción.
Pankhurst, R.J., Rapela, C.W., Fanning, C.M., Márquez, M., 2006. Gondwanide continental collision and the origin of Patagonia. Earth-Sci. Rev. 76, 235–257.
Paredes, J.M., Giacosa, R.E., Heredia, N., 2009. Sedimentary evolution of Neogene continental deposits (Ñirihuau Formation) along the Ñirihuau River, North Patagonian Andes of Argentina. J. S. Am. Earth Sci. 28 (1), 74–88.

Please cite this article as: Tobal, J.E., et al., Middle to late Miocene extensional collapse of the North Patagonian Andes (41°30′–42°S), Tectonophysics (2015), http://dx.doi.org/10.1016/j.tecto.2015.06.032

Parra, M., Mora, A., Lopez, C., Rojas, L.E., Horton, B.K., 2012. Detecting earliest shortening and deformation advance in thrust belt hinterlands: example from the Colombian Andes. Geology 40, 175–178.
Pearson, D.M., Kapp, P., DeCelles, P.G., Reiners, P.W., Gehrels, G.E., Ducea, M.N., Pullen, A., 2013. Influence of pre-Andean crustal structure on Cenozoic thrust belt kinematics and shortening magnitude: Northwestern Argentina. Geosphere 9 (6), 1766–1782.
Pécskay, Z., Haller, M.J., Németh, K., 2007. Preliminary K/Ar geochronology of the Crater Basalt volcanic field (CBVF), northern Patagonia. Rev. Asoc. Geol. Argent. 62 (1), 25–29.
Ponza, A., Pazzaglia, F.J., Picotti, V., 2010. Thrust-fold activity at the mountain front of the Northern Apennines (Italy) from quantitative landscape analysis. Geomorphology 123, 211–231.
Rabassa, J., Evenson, E.B., Stephens, G.C., 1986. Nuevas evidencias del englazamiento Plioceno–Peistoceno inferior en los Andes Patagónicos Septentrionales: Cerro Tronador, Río Negro. Rev. Asoc. Geol. Argent. 41 (3-4), 405–409.
Ramos, V.A., Cortés, J., 1984. Estructura e interpretación tectónica. In: Ramos, V.A. (Ed.), Geología y Recursos Naturales de la Provincia de Río Negro, I (12), 317–346 (Buenos Aires).
Ramos, M.E., Forestier, J., Folguera, A., Giménez, M., Ramos, V.A., 2014. Evolución de los Andes Nordpatagónicos a la altura del río Cushamen a partir del estudio de las formaciones Ñirihuau y Collón Cura. XIX Congreso Geológico Argentinopp. S22–S55 (Córdoba).
Rapela, C.W., Spalletti, L., Merodio, J.C., 1983. Evolución magmática y geotectónica de la Serie Andesitica andina (Paleoceno–Eoceno) en la cordillera norpatagónica. Rev. Asoc. Geol. Argent. 38 (3-4), 469–484.
Rapela, C., Munizaga, F., Dalla Salda, L., Hervé, F., Parada y, M., Cingolani, C., 1987. Nuevas edades K–Ar de los granitoides del sector nororiental de los Andes Patagónicos. X Congreso Geológico Argentino. 4, pp. 18–20 (Tucumán.).
Rapela, C., Spalletti, L., Merodio, J., Aragón, E., 1988. Temporal evolution and spatial variation of early Tertiary volcanism in the Patagonian Andes (40°S–42°30′S). J. S. Am. Earth Sci. 1 (1), 75–88.
Rapela, C.W., Pankhurst, R.J., Fanning, C.M., Hervé, F., 2005. Pacific subduction coeval with the Karoo mantle plume: the Early Jurasssic Subcordilleran belt of northwestern Patagonia. Geol. Soc. Lond., Spec. Publ. 246 (1), 217–239.
Rossetti, F., Faccenna, C., Ranalli, G., 2002. The influence of backstop dip and convergence velocity in the growth of viscous doubly vergent orogenic wedges: Insights from thermomechanical laboratory experiments. J. Struct. Geol. 24, 953–962.
Sellés, D., Moreno, H., 2011. Geología del volcán Calbuco (1:50.000). Servicio Nacional de Geología y Minería, SERNAGEOMIN, Carta Geológica de Chile. 130 p. 38 (Santiago).
Sepúlveda, E.G., Viera, R.M., 1980. Geología y área de alteración en el cerro Colorado y alrededores, Chubut noroccidental. Rev. Asoc. Geol. Argent. 35 (2), 195–202.
SERNAGEOMIN-BRGM, 1995. Carta Metalogénica X Región Sur, Chile. Servicio Nacional de Geología y Minería-Bureau de Recherches Géologiques et Minières, Informe Registrado IR-95-05. 10 (Santiago, Chile).
Siebert, L., Simkin, T., 2002. Volcanoes of the World: An Illustrated Catalog of Holocene Volcanoes and their Eruptions. Smithsonian Institution. Global Volcanism Program Digital Information Series, GVP-3http://www. volcano. si. edu/world/.
Somoza, R., Ghidella, M.E., 2012. Late Cretaceous to recent plate motions in western South America revisited. Earth Planet. Sci. Lett. 331–332, 152–163.
Sternai, P., Herman, F., Fox, M.R., Castelltort, S., 2011. Hypsometric analysis to identify spatially variable glacial erosion. J. Geophys. Res. 116. http://dx.doi.org/10.1029/2010JF001823.
Sternai, P., Herman, F., Champagnac, J.D., Fox, M., Salcher, B., Willet, S.D., 2012. Pre-glacial topography of the European Alps. Geology 40 (12), 1067–1070.
Sternai, P., Jolivet, L., Menant, A., Gerya, T., 2014. Driving the upper plate surface deformation by slab rollback and mantle flow. Earth Planet. Sci. Lett. 405, 110–118.
Strecker, M.R., Alonso, R.N., Bookhagen, B., Carrapa, B., Hilley, G.E., Sobel, E.R., Trauth, M.H., 2007. Tectonics and climate of the southern central Andes. Annu. Rev. Earth Planet. Sci. 35, 747–787.
Strecker, M.R., Alonso, R., Bookhagen, B., Carrapa, B., Coutand, I., Hain, M.P., Hilley, G.E., Mortimer, E., Schoenbohm, L., Sobel, E.R., 2009. Does the topographic distribution of the central Andean Puna Plateau result from climatic or geodynamic processes? Geology 37 (7), 643–646.
Suárez, M., De La Cruz, R., Bell, M., 1996. Estratigrafía de la región de Coihaique (latitud 45°–46°S); Cordillera Patagónica, Chile. XIII Congreso Geológico Argentino. I pp. 575–590 (Buenos Aires).
Suárez, M., Emparán, C., 1997. Hoja Curacautín. Regiones de la Araucanía y del Bio-Bio (1: 250.000). Servicio Nacional de Geología y Minería. SERNAGEOMIN, Carta Geológica de Chile, Santiago, pp. 1–105 (71 pp.).
Tagiri, M., Moreno, H., López-Escobar, L., Notsu, K., 1993. Two types of the high-alumina basalt series of Osorno Volcano, Southern Andes (41°06′S)-plagioclase dilution effect. J. Mineral. Pet. Econ. Geol. 88 (7), 359–371.
Thiele, R., Castillo, J.C., Hein, R., Romero, G., Ulloa, M., 1978. Geología del sector fronterizo de Chiloé continental entre los 43°–43°45′ latitud sur, Chile (columnas de Futaleufú y Palena). VII Congreso Geológico Argentino. I pp. 577–591 (Neuquén).
Thomson, S.N., 2002. Late Cenozoic geomorphic and tectonic evolution of the Patagonian Andes between latitudes 42° S and 46° S: an appraisal based on fission track results from the transpressional intra-arc Liquiñe–Ofqui fault zone. Geol. Soc. Am. Bull. 114 (9), 1159–1173.
Thomson, S., Brandon, M., Tomkin, J., Reiners, P., Vásquez, C., Wilson, N., 2010. Glaciation as a destructive and constructive control on mountain building. Nature 467, 213–317.
Tibaldi, A., 2008. Contractional tectonics and magma paths in volcanoes. J. Volcanol. Geotherm. Res. 176, 291–301.
Tibaldi, A., Corazzato, C., Rovida, A., 2009. Miocene–Quaternary structural evolution of the Uyuni–Atacama region, Andes of Chile and Bolivia. Tectonophysics 471, 114–135.
Tibaldi, A., Pasquarè, F.A., Tormey, D., 2010. Volcanism in reverse and strike-slip fault settings. In: Negendank, J. (Ed.), S. Cloetingh. Springer-Verlag, New Frontiers in Integrated Solid Earth Sciences, pp. 315–348.
Tobal, J.E., Rojas Vera, E., Folguera, A., Ramos, V.A., 2012. Deformación andina en el cordón del Hielo Azul al oeste de El Bolsón: implicancias en la evolución tectónica de la Cordillera Norpatagónica en Río Negro, Argentina. Andean Geol. 39 (3), 442–463.
Valla, P.G., Shuster, D.L., van der Beek, P.A., 2011. Significant increase in relief of the European Alps during mid-Pleistocene glaciations. Nat. Geosci. 4, 688–692.
Varela, R., Basei, M., Cingolani, C., Siga Jr., O., Passarelli, C., 2005. El basamento cristalino de los Andes norpatagónicos en Argentina: geocronología e interpretación tectónica. Rev. Geol. Chile 32 (2), 167–187.
Vargas, G., Rebolledo, S., Sepúlveda, S.A., Lahsen, A., Thiele, R., Townley, B., Padilla, C., Rauld, R., Herrera, M.J., Lara, M., 2013. Submarine earthquake rupture, active faulting and volcanism along the major Liquiñe–Ofqui Fault Zone and implications for seismic hazard assessment in the Patagonian Andes. Andean Geol. 40 (1), 141–171.
Vergara, M., Muñoz, J., 1982. La Formación Cola de Zorro en la Alta cordillera Andina Chilena (36°–39°S), sus características petrográficas y petrológicas: una revisión. Rev. Geol. Chile 17, 31–46.
Wang, W.H., Davis, D.M., 1996. Sandbox model simulation of forearc evolution and noncritical wedges Journal of Geophysical Research 101, 11329–11339.
Watt, S.F.L., 2010. Records of volcanism and controls on volcanic processes in southern Chile (D.Phil thesis), Department of Earth Sciences, University of Oxford, U.K., p. 367 (http://ora.ouls.ox.ac.uk/).
Watt, S.F.L., Pyle, D.M., Mather, T.A., 2011. Geology, petrology and geochemistry of the dome complex of Huequi volcano, southern Chile. Andean Geol. 38 (2), 335–348.
Wells, M.L., Hoisch, T.D., 2008. The role of mantle delamination in widespread late Cretaceous extension and magmatism in the Cordilleran orogen, western United States. Geol. Soc. Am. Bull. 120, 515–530.
Wells, M.L., Hoisch, T.D., Cruz-Uribe, A.M., Vervoort, J.D., 2012. Geodynamics of synconvergent extension and tectonic mode switching: constraints from the Sevier–Laramide orogen. Tectonics 31 (TC1002).
Whipple, K.X., 2009. The influence of climate on the tectonic evolution of mountain belts. Nat. Geosci. 2, 97–104.
Willet, S., 1999. Rheological dependence of extension in wedge models of convergent orogens. Tectonophysics 305, 419–435.
Yrigoyen, M., 1969. Problemas estratigráficos del Terciario en la Argentina. Ameghiniana 6 (4), 315–329.

Please cite this article as: Tobal, J.E., et al., Middle to late Miocene extensional collapse of the North Patagonian Andes (41°30′–42°S), Tectonophysics (2015), http://dx.doi.org/10.1016/j.tecto.2015.06.032